Hyperfine effects in the nuclear magnetic resonance of paramagnetic molecules

Dissertation for the degree of Doctor Philosophiae

Teemu Pennanen
University of Helsinki
Faculty of Science
Department of Chemistry
Laboratory of Physical Chemistry
P.O. Box 55 (A.I. Virtasen aukio 1)
FI-00014 University of Helsinki, Finland

To be presented, with the assent of the University of Helsinki for public discussion in Auditorium A110, Department of Chemistry (A. I. Virtasen aukio 1, Helsinki), August the 23rd, 2011, at noon.

Helsinki 2011

Supervised by

Prof. Juha Vaara
Department of Physics
University of Oulu
Oulu, Finland

Reviewed by

Dr. Perttu Lantto
Department of Physics
University of Oulu
Oulu, Finland

Prof. Frank Neese
Institute for Physical and Theoretical Chemistry
Universität Bonn
Bonn, Germany

Opponent

Prof. Michael Bühl
School of Chemistry
University of St Andrews
St Andrews, United Kingdom

ISBN 978-952-10-7106-5 (Paperback)
ISBN 978-952-10-7107-2 (PDF)
http://ethesis.helsinki.fi
Yliopistopaino Helsinki 2011

Abstract

Paramagnetic, or open-shell, systems are often encountered in the context of metalloproteins, and they are also an essential part of molecular magnets. Nuclear magnetic resonance (NMR) spectroscopy is a powerful tool for chemical structure elucidation, but for paramagnetic molecules it is substantially more complicated than in the diamagnetic case. Before the present work, the theory of NMR of paramagnetic molecules was limited to spin-1/2 systems and it did not include relativistic corrections to the hyperfine effects. It also was not systematically expandable.

The theory was first expanded by including hyperfine contributions up to the fourth power in the fine structure constant α. It was then reformulated and its scope widened to allow any spin state in any spatial symmetry. This involved including zero-field splitting effects. In both stages the theory was implemented into a separate analysis program. The different levels of theory were tested by demonstrative density functional calculations on molecules selected to showcase the relative strength of new NMR shielding terms. The theory was also tested in a joint experimental and computational effort to confirm assignment of ^{11}B signals.

The new terms were found to be significant and comparable with the terms in the earlier levels of theory. The leading-order magnetic-field dependence of shielding in paramagnetic systems was formulated.

The theory is now systematically expandable, allowing for higher-order field dependence and relativistic contributions. The prevailing experimental view of pseudocontact shift was found to be significantly incomplete, as it only includes specific geometric dependence, which is not present in most of the new terms introduced here. The computational uncertainty in density functional calculations of the Fermi contact hyperfine constant and zero-field splitting tensor sets a limit for quantitative prediction of paramagnetic shielding for now.

Keywords: ESR, NMR, paramagnetic, DFT, molecular properties, magnetic properties

Acknowledgements

The research for the present work was performed at the Laboratory of Physical Chemistry in the Department of Chemistry at the University of Helsinki, between 2004 and 2010. I would like to express my gratitude for being able to work in such a stimulating environment. Among the excellent staff there, I am especially grateful to Profs. Lauri Halonen and Markku Räsänen for their support during the years.

Financial support of the Emil Aaltonen foundation, Jenny and Antti Wihuri fund, Finnish Chemical Society, the LASKEMO graduate school and the research funds of the University of Helsinki is gratefully acknowledged. The computing resources provided by CSC (Espoo) and the Departments of Chemistry and Physical Sciences at UH were essential for the completion of the work.

I would like to thank my supervisor, Prof. (then Docent and university lecturer) Juha Vaara, foremost for having saint-like patience when the work didn't proceed as expected, and for being an exemplary scientist and an excellent boss. It has truly been an honour to work with you.

To all my coworkers and scientific collaborators, thank you for all the discussions, on science and otherwise. Especially Juho Lintuvuori, Ville Weijo, Matti Hanni, Teemu S. Pennanen, Jouni Karjalainen, Pekka Manninen, Michal Straka, Stefan Taubert and Prof. Martin Kaupp. Special thanks go to the reviewers of this thesis, Perttu Lantto and Prof. Frank Neese, as well as to Prof. Lauri Halonen for his comments.

To my parents, Päivi and Mauri, it is impossible to thank you enough for everything you have done, and still continue to do for me, so I will settle for

a simple "Kiitos".

To my friends, Janne, Jere, Hannu, Esa, Hanna, SP, Keijo, Ville, Jelena, Akseli, Petri, Antti, Michael, Mikko, Reijo, Matti, Elina, Teemu, Ilmo, Arno, Jouni, HYK and everyone I have forgotten to mention, thank you for providing me with the balance between work and fun, and all the joyful moments throughout the years. And a moment of remembrance to those who are no longer among us.

To my fiancée, Kaisa, special thanks. You give meaning to this work and without you, it would never have been finished.

Berlin, June 2011
Teemu Pennanen

List of publications

Publications included in the thesis

I: T.O. Pennanen and J. Vaara, *Density-functional calculations of relativistic spin-orbit effects on nuclear magnetic shielding in paramagnetic molecules*, Journal of Chemical Physics **123**, 174102:1-10 (2005).
II: T.O. Pennanen and J. Vaara, *Nuclear magnetic resonance chemical shift in an arbitrary electronic spin state*, Physical Review Letters **100**, 133002:1-4 (2008).
III: H. Liimatainen, T.O. Pennanen and J. Vaara, ^{1}H *Chemical shifts in non-axial, paramagnetic chromium(III) complexes: Application of novel pNMR shift theory*, Canadian Journal of Chemistry **87**, 954-964 (2009).
IV: T.O. Pennanen, J. Macháček, S. Taubert, J. Vaara and D. Hnyk, *Ferrocene-like iron bis(dicarbollide), [3-Fe^{III}-(1,2-$C_2B_9H_{11}$)$_2$]$^-$. The First Experimental and Theoretical Refinement of a Paramagnetic ^{11}B NMR Spectrum*, Physical Chemistry Chemical Physics **12**, 7018-7025 (2010).

The author did all the programming required for the included works, and performed all the calculations in Papers I, II and IV. The author participated in the development of the theory in Paper II. The initial drafts of Papers I and IV were prepared by the author. All the papers were finalized as teamwork.

Other publications not included in the thesis

A: O. Laakso, T. Pennanen, K. Himberg, T. Kuitunen, J.-J. Himberg, *Effect of eight solvents on ethanol analysis by Dräger 7110 Evidential breath analyzer*, Journal of Forensic Sciences **49**(5), 1113-1116 (2004).

B: O. Laakso, M. Haapala, T. Pennanen, T. Kuitunen and J.-J. Himberg, *Fourier-transformed infrared breath testing after ingestion of technical alcohol*, Journal of Forensic Sciences **52**(4), 982-987 (2007).

C: S. Taubert, M. Straka, T.O. Pennanen, D. Sundholm and J. Vaara, *Dynamics and magnetic resonance properties of* $Sc_3C_2@C_{80}$ *and its monoanion*, Physical Chemistry Chemical Physics **10**, 7158-7168 (2008).

D: J. Mares, H. Liimatainen, T.O. Pennanen and J. Vaara, *Magnetic properties of* $Ni^{2+}(aq)$ *from first principles*, submitted for publication.

List of Abbreviations

AMFI	Atomic Mean Field
B3LYP	(Becke's three-parameter exchange)-Lee-Yang-Parr hybrid functional
BHandHLYP	(Becke's Half-and-Half exchange)-Lee-Yang-Parr hybrid functional
BLYP	Becke-Lee-Yang-Parr GGA functional
BOA	Born-Oppenheimer Approximation
BP86	Becke-Perdew 1986 GGA functional
CPKS	Coupled-perturbed Kohn-Sham
DFT	Density Functional Theory
ECP	Effective Core Potential
EPR	Electron Paramagnetic Resonance
ESR	Electron Spin Resonance
FC	Fermi Contact
GGA	Generalized Gradient Approximation
HF	Hartree-Fock (method)
MD	Molecular Dynamics

NMR	Nuclear Magnetic Resonance
PBE	Perdew-Burke-Ernzerhof GGA functional
PBE0	Perdew-Burke-Ernzerhof hybrid functional
PC	Pseudocontact
pNMR	paramagnetic NMR
PW91	Perdew-Wang 1991 GGA functional
RI-J DFT	Resolution of Identity in Coulomb (J) integrals DFT method
RI-JK DFT	Resolution of Identity in Coulomb (J) and exchange (K) integrals DFT method
SO	Spin-orbit
ZFS	Zero-field Splitting

Contents

Chapter 1

Introduction

The nuclei of most atoms can be described as magnets. Such nuclei are said to have non-zero spin (see section 2.2). In analogy to a classical magnetic dipole, in an external magnetic field the direction of the nuclear spin precesses around the direction of the external field, and the average nuclear magnetic moment is either parallel or antiparallel to the external field. Photons of a radio frequency typical for the nucleus and also dependent on the strength of the external magnetic field can excite the nuclei from a lower-energy state to a higher-energy state. After a characteristic period of time (varying roughly in the range of 10^{-11} s... 10^{4} s), the excitation of the system relaxes and photons are emitted. This phenomenon is called nuclear magnetic resonance (NMR).

Usually, nuclei are surrounded by other nuclei and electrons. This changes the resonance energy difference, and the nucleus is said to be shielded (for a resonance at lower frequency than for a bare nucleus) or de-shielded (for a resonance at higher frequency). The effective magnetic field $\boldsymbol{B}_K$ interacting with the nucleus K can be written as

$$\boldsymbol{B}_K = (\mathbf{1} - \boldsymbol{\sigma}_K) \cdot \boldsymbol{B}_0, \tag{1.1}$$

where $\boldsymbol{\sigma}_K$ is the nuclear shielding tensor of nucleus K, usually measured in parts per million (ppm) of the bare nucleus resonance frequency, and $\boldsymbol{B}_0$ is the external magnetic field. Nuclear shielding is specific for different nuclei in

different chemical compounds. Since its invention in 1946 by Felix Bloch and Edward Purcell [1, 2, 3], NMR spectroscopy has become a powerful tool for structure elucidation in chemistry [4]. Another important application of the phenomenon is magnetic resonance imaging (MRI) [4], used in medicine and materials science. In MRI, the differing spectroscopic properties of parts of bulk matter are utilized to form images without the use of ionizing radiation inherent in, *e.g.*, X-ray imaging.

In a measurement of a macroscopic sample, the nuclear shielding $\boldsymbol{\sigma}$ is motionally averaged. This includes tumbling of the molecules, rotation of single bonds and internal vibrations. Due to this averaging, the observed σ in liquid or gaseous phase is a single, isotropic value for geometrically equivalent atoms, *e.g.*, the hydrogens in a methyl group. The anisotropy of the shielding tensor can be measured for molecules suspended into solid phase or liquid crystals. When the measured σ is subtracted from the shielding of the same atom species in a reference compound σ_{ref}, the result is called the chemical shift δ, which is defined as

$$\delta = \frac{\sigma_{\text{ref}} - \sigma}{1 - \sigma_{\text{ref}}} \approx \sigma_{\text{ref}} - \sigma, \tag{1.2}$$

where the approximation holds when σ_{ref} is small. The origin of the chemical shift scale is set to a specific NMR signal from the reference compound. The most common chemical shift reference compound for ^{1}H and ^{13}C NMR spectroscopy is tetramethylsilane [TMS, $Si(CH_3)_4$].

The nuclear magnetic moments also interact with each other, both directly and via the electronic structure. This coupling is weak compared to the chemical shift, and it is mostly interesting due to the characteristic splitting of the spectral peaks it causes. For paramagnetic systems, the peaks are usually so broad that their splitting structure cannot be observed [5], and thus this work concentrates on the chemical shifts. Even for molecules as large as proteins with thousands of atoms, meaningful measurements can be made and it is in principle possible to find a one-to-one correlation between the structure of the molecule and its NMR spectrum. This work often requires both a lot of time and expensive machinery. To help make their use more effi-

cient, methods for the prediction of an NMR spectrum based on a suggested molecular structure have been developed. The methods for solving this inverse problem range from relatively simple lookup tables of chemical shifts for functional groups and modifications to these shifts from the surrounding atoms [6], to computational methods based on first principles electronic structure calculations [7, 8, 9], the topic of this work. First principles methods for spectral prediction try to achieve their goal with as few assumptions as possible. These start from the basic postulates of quantum mechanics to obtain the approximate electronic structure of the system. The laws defining the spectral parameters are formulated for a general, system-independent case, and then the rules are applied on the approximate state obtained. From these parameters, the NMR spectrum can be reconstructed. Obtaining NMR properties from electronic structure calculation can give valuable insight to the phenomenological basis behind the observed values. It can also act as a way of calibrating the electronic structure calculation methods themselves, to ensure they give correct results for the correct reason instead of relying on error cancellation.

For diamagnetic systems, *i.e.*, those without any unpaired electrons, the methods for the prediction of chemical shifts are well-established and reasonably reliable for even quantitative work [8, 9]. For paramagnetic systems, such as main group radicals and most transition metal complexes, only recently there has been a method [10] that would include more than the most basic contributions as outlined by McConnell in 1958 [11, 12]. The existing consistent theories including that developed by Moon and Patchkovskii [10] were also limited to systems with only one unpaired electron (doublet systems), which further limited their usefulness.

As several important molecules, *e.g.*, proteins and molecular magnets, have one or more paramagnetic metal centres, a reliable method for the prediction of paramagnetic NMR (pNMR) spectra would be useful. An example of such a system is the four-manganese centre in the oxygen evolving complex of photosystem II, which is responsible for the production of gaseous oxygen

in cyanobacteria and green plants [13, 14]. The value is further increased because unlike the most-used tool for protein structure determination, X-ray crystallography, NMR can be used for proteins that are still active in the aqueous phase [15]. Another important use for paramagnetic compounds is as transition metal-containing catalysts in chemical industry [16].

The aim of this work is to improve the theoretical understanding of pNMR shifts, to develop computational methods based on the new theoretical framework created, and to apply them on representative molecules to demonstrate the new shielding terms introduced by the changes to the theory. In Paper I, the doublet theory was reformulated based on the work of Moon and Patchkovskii [10], and a spin-orbit contribution to the hyperfine coupling was added to the calculation. The computational methods were implemented into the deMon suite of quantum chemistry software [17], and tested on a main-group radical studied earlier by Rinkevicius *et al.* [18] and the first 3 cobalt group metallocenes ($CoCp_2$, $RhCp_2$, $IrCp_2$), with comparison to earlier experimental results [19, 20, 21, 22, 23, 24]. This was the first consistent implementation of a theory based on the ideas of Moon and Patchkovskii, as well as the first time that the hyperfine spin-orbit effects were consistently included in chemical shift calculations.

In Paper II, the theory was further expanded to allow any spin state of the molecule. A completely new program was written to allow the use of any available property code to obtain the required orbital shielding and electron spin resonance (ESR) property tensors. The program was tested with the set of metallocenes also used by Hrobárik *et al.* [25] to test their *a posteriori* theory for systems with more than one unpaired electron. The theory presented by Hrobárik *et al.* used the magnetic susceptibility as an intermediate variable to obtain the chemical shifts, as is the usual practice in experimental studies. It was also limited to axially symmetric systems, unlike the general theory presented in Paper II. The metallocene results were compared to computational and experimental values listed in ref. [25]. In Paper II the new theory was also tested on a chiral chromium complex,

along with a formulation for the leading-order magnetic field-dependence of NMR shielding.

In Paper III, a set of quinolyl-functionalized Cp chromium(III) complexes, precursors of olefine synthesis catalysts, was studied with the methods of Paper II and the results were compared with ones obtained without the additions introduced in Papers I and II, and also with the experimental results in ref. [16]. The chromium complexes in Papers II and III have total electron spin $S > \frac{1}{2}$. These species are not axially symmetric so that the magnitude of the new terms introduced in Paper II could be evaluated.

In Paper IV, a metallocarborane system was studied with the methods of Paper I using the software developed in Paper II. First-principles results were for the first time used to confirm the assignment of experimental paramagnetic ^{11}B signals. The effects of a non-static molecular geometry on the ^{11}B chemical shifts were estimated by a molecular dynamics (MD) simulation. Solvent effects were included using the COSMO [26] model.

Chapter 2

Main concepts

2.1 Quantum mechanics

In the macroscopic scale, measured physical quantities can obtain any value in a continuum. When observed on a small enough scale, these are quantized, and can have only certain values dependent on the system. For example, the electrons in an atom can only have certain energy levels. These systems absorb and emit quanta of electromagnetic radiation, photons, in transitions between these energy levels. For the same transition, the energy of these photons and, thus, also their wavelength, is always the same. This idea of quantization was first postulated by Planck in 1901 for the energy levels of blackbody radiation [27], then expanded to electromagnetic radiation itself by Einstein in his explanation of the photoelectric effect in 1905 [28]. In 1926, Schrödinger formulated this as the time-independent equation,

$$H\Psi = E\Psi, \tag{2.1}$$

a stationary special case of his wave function formalism [29, 30, 31, 32]. It states that the allowed energy levels of a system described by the operator H, the Hamiltonian, are given as the eigenvalues E, when it operates on its eigenfunctions Ψ. In Heisenberg's matrix mechanics formulation of quantum mechanics, these are called the eigenstates [33, 34, 35]. In the Copenhagen interpretation, the squared norm of the wave function is interpreted as a

probability density. If a wave function describes an electron in an atom, its squared norm integrated over a volume describes the probability of finding the electron inside that volume at a given moment.

Any system is fully described by its Hamiltonian and the corresponding solutions to Schrödinger's equation. The only, and greatest hurdle, remaining to this day is actually obtaining the solution of the equation, as famously stated by Dirac already in 1929.* [36]

2.2 Spin

Spin is one of the fundamental properties used to categorize particles. In the atomic unit system† it obtains dimensionless values of zero or higher at $\frac{1}{2}$ intervals. It is a true quantum mechanical property, not found in macroscopic objects, which behaves like an intrinsic angular momentum with an associated magnetic dipole. A particle with spin behaves like a rotating charged object, hence the name "spin", but this picture of a rotating charge breaks down for point-like particles such as the electron, for which the concept of rotation is ill-defined. The interaction of a particle spin with an external magnetic field causes splitting of the energy levels in the system. This is called the Zeeman effect, and it forms the basis for the NMR and ESR methods as well as an integral part of Mössbauer spectroscopy. [37]

2.2.1 Nuclear magnetic resonance

The energy levels of a particle with spin $s = \frac{n}{2}$ are Zeeman-split into $n + 1$ states each. These states have a magnetic spin quantum number m_s ranging from $-\frac{n}{2}$ to $\frac{n}{2}$ at unit intervals. Thus, a spin-$\frac{1}{2}$ particle such as the proton or

*"The underlying physical laws necessary for the mathematical theory of a large part of physics and the whole of chemistry are thus completely known, and the difficulty is only that the exact application of these laws leads to equations much too complicated to be soluble."

†In the SI-based atomic unit system, used throughout this work unless otherwise stated, $\hbar = m_e = 4\pi\epsilon_0 = e = 1$, $c = \alpha^{-1} \approx 137$.

the electron has the spin states $m_s = \frac{1}{2}$ and $m_s = -\frac{1}{2}$, usually labelled α and β. The energy difference between the states is $\Delta E = g\mu_\mathrm{B}B_0 = gB_0/2$, where g is the g-factor of the particle (for a free electron $g = g_e = 2.002319$ [38], for nuclei the absolute value of g is on the order of $10^{-4} \ldots 10^{-2}\ g_e$ [39]) and $\mu_\mathrm{B} = e\hbar/2m_e = 1/2$ is the Bohr magneton. For nuclei in atoms, solids and molecular systems, the change in resonance frequency ν from that of a bare nucleus arises from interaction with the electron cloud affected by an external magnetic field [actual shielding $\boldsymbol{\sigma}$, see Eq. (1.2)], interaction with other nuclei in the system (spin-spin coupling) directly ($\boldsymbol{D}_{KL}$) and indirectly ($\boldsymbol{J}_{KL}$). In the case of $S > 1/2$ nuclei, there is also interaction of the nuclear quadrupole moment with the electric field gradient (quadrupole coupling $\boldsymbol{\mathcal{B}}$). [40]

2.2.2 Electron spin resonance

Electron Spin Resonance (ESR) is similar to NMR, but it deals with unpaired electrons in addition to nuclei, usually in radicals and metal complexes [5]. It is also called electron paramagnetic resonance (EPR) in the case of transition metal complexes where spin-orbit effects are strong. The principal measured quantities in ESR spectroscopy are the g-tensor of the effective electronic spin [40] describing the coupling of the unpaired electron spin to the external magnetic field, the hyperfine coupling $\boldsymbol{A}_K$ of nuclear spin to the electron spin, and zero-field splitting $\boldsymbol{D}$, which arises from the coupling of effective electron spin with itself. The difference of rotationally averaged isotropic g value from the free electron value g_e arises from interactions between the effective electron spin and its surroundings. In the present approximation, this includes the spin-orbit and orbital Zeeman effects as well as relativistic kinetic energy corrections to the spin-Zeeman interaction, see section 3.2 for details. The coupling $\boldsymbol{A}_K$ measures the interaction of the effective electron spin to the spin of the nucleus K. Zero-field splitting $\boldsymbol{D}$ parameterizes the splitting of the electron spin states caused by the coupling of unpaired electron spins to each other. Unlike the splitting caused by $\boldsymbol{A}$, the zero-field

splitting is independent of the external magnetic field, hence the name.

2.3 Electronic structure calculations

Of the tools used to obtain approximate solutions of the Schrödinger equation for chemical systems, one of the earliest, and still the one used most is the Born-Oppenheimer approximation (BOA) [41]. The kinetic energy of the nuclei is estimated to be negligible by assuming the electron-nucleus mass ratio to be very small. This allows the separation of the electronic wavefunction Ψ_e from the nuclear one. In addition to making electronic structure calculations simpler, BOA allows tracing of potential energy surfaces by changing the nuclear coordinates [42].

Approximate solutions of the Schrödinger equation for the electronic Hamiltonian are often obtained by the Hartree-Fock (HF) method. It starts by first factorizing the N-electron wave function Φ into a product of N one-electron wave functions $\phi_i(\boldsymbol{x}) = \phi_i(\boldsymbol{r}, \boldsymbol{\sigma})$ in coordinates $\boldsymbol{x}$ which are composed of spatial ($\boldsymbol{r}$) and spin ($\boldsymbol{\sigma}$) parts. These wave functions are also called molecular spin orbitals (MO). Then, an $N \times N$ determinant is formed, where each of the one-electron wave functions is combined with each electronic coordinate,

$$\Phi(\boldsymbol{x}_1, \boldsymbol{x}_2, \ldots, \boldsymbol{x}_N) = \frac{1}{\sqrt{N!}} \begin{vmatrix} \phi_1(\boldsymbol{x}_1) & \phi_2(\boldsymbol{x}_1) & \ldots & \phi_N(\boldsymbol{x}_1) \\ \phi_1(\boldsymbol{x}_2) & \phi_2(\boldsymbol{x}_2) & \ldots & \phi_N(\boldsymbol{x}_2) \\ \vdots & \vdots & \ddots & \vdots \\ \phi_1(\boldsymbol{x}_N) & \phi_2(\boldsymbol{x}_N) & \ldots & \phi_N(\boldsymbol{x}_N) \end{vmatrix}. \tag{2.2}$$

This Slater determinant presentation of the wave function has the antisymmetry properties required by the Pauli exclusion principle, which states that the wave function should change sign but remain otherwise unchanged in the exchange of two electrons. This corresponds to exchange of two rows in the determinant. Also, two electrons cannot be in exactly the same state, as the determinant would be zero. The electronic energy of the N-electron system

can be written as

$$\begin{aligned} E = \langle \Phi \left| H \right| \Phi \rangle &= \sum_i \langle \phi_i \left| h \right| \phi_i \rangle + \frac{1}{2} \sum_{i,j} \langle \phi_i \left| J_j - K_j \right| \phi_i \rangle \\ &= \sum_i \langle \phi_i \left| h \right| \phi_i \rangle \\ &+ \frac{1}{2} \sum_{i,j} \left\langle \phi_i \phi_j \left| \frac{1}{r_{12}} \right| \phi_i \phi_j \right\rangle - \frac{1}{2} \sum_{i,j} \left\langle \phi_i \phi_j \left| \frac{1}{r_{12}} \right| \phi_j \phi_i \right\rangle , \end{aligned} \tag{2.3}$$

where J is the Coulomb operator, K is the exchange operator, Φ is the Slater determinant and h is the one-electron operator including kinetic energy and nuclear attraction. In the two-electron integrals r_{12} is the distance between the spatial integration coordinates associated with electrons 1 and 2.

Introducing an infinitesimal variation to the MOs, $\phi_i \Rightarrow \phi_i + \delta\phi_i$, we can find the corresponding variation in energy, which is to the leading order [43]

$$\begin{aligned} \delta^{(1)} E[\Phi] &= \sum_i \langle \delta\phi_i \left| h \right| \phi_i \rangle + \sum_{i,j} \langle \delta\phi_i \left| J_j - K_j \right| \phi_i \rangle + \text{c.c.} \\ &= \sum_i \langle \delta\phi_i \left| F \right| \phi_i \rangle + \text{c.c.} \end{aligned} \tag{2.4}$$

where the Fock operator $F = h + \sum_j (J_j - K_j)$ and c.c. denotes complex conjugate. According to the variational principle, to minimize the energy with respect to changes in molecular orbitals, the variation in energy must vanish. This implies that at the minimum energy,

$$\langle \delta\phi_i \left| F \right| \phi_i \rangle = 0 \tag{2.5}$$

for any variation that obeys the orthonormality constraint, $\langle \phi_i | \phi_j \rangle = \delta_{ij}$ where δ_{ij} is the Kronecker delta. When such a variation is expanded as a linear combination of the MOs and the expansion coefficient matrix is diagonalized in the MO basis, we obtain the canonical HF equations,

$$F \left| \phi_i \right\rangle = \epsilon_i \left| \phi_i \right\rangle . \tag{2.6}$$

The orbitals ϕ_i can be expanded as linear combinations of basis functions η,

$$\phi_i = \sum_j C_i^j \eta_j , \tag{2.7}$$

vide infra, p. 15. Because these basis functions are centred on the nuclei, these functions are called atomic orbitals (AO), this is called the LCAO (linear combination of atomic orbitals) expansion. Alternatively, plane waves can be used for the expansion, and these are a popular choice for large and periodic systems, especially in solid state physics and surface chemistry. In the LCAO formalism, the Schrödinger equation is written in matrix form with the expansion coefficients as variables. These are called the Roothaan-Hall equations [44, 45],

$$\boldsymbol{FC} = \boldsymbol{SC}\boldsymbol{\epsilon}. \tag{2.8}$$

Here, $\boldsymbol{F}$ is the Fock matrix corresponding to the electronic Hamiltonian of the system, $\boldsymbol{C}$ is the MO coefficient matrix, $\boldsymbol{S}$ is the overlap matrix between the atomic orbitals, and $\boldsymbol{\epsilon}$ is a diagonal matrix containing the MO energies. In the self-consistent field (SCF) method, an initial guess of $\boldsymbol{C}$ is first constructed. Then, cycles consisting of constructing the Fock matrix and diagonalizing it to obtain a new set of coefficients $\boldsymbol{C}$ are repeated until specified convergence criteria are reached. Usually thresholds for both the change in the total energy and the coefficients are used. It should be noted that in the SCF method the many-body problem of n electrons is turned into n one-body problems, each of the electrons interacting with the average field of the nuclei and the other electrons.

HF is the basis of most wave function-based methods for electronic structure calculations, but it lacks in its description an important phenomenon, electron correlation. Electrons repel each other, both due to their electric charge and due to purely quantum mechanical reasons. Hence, the probability densities of their locations are correlated. The HF method includes Fermi correlation, which is caused by the non-Coulomb repulsion between electrons with parallel spins, as per Pauli exclusion principle. As the HF method only models average Coulomb repulsion between one-electron charge distributions, Coulomb correlation caused by the electrostatic Coulomb repulsion between electrons is not included. A direct consequence of electron correlation is Hund's rule [42]. It states that the configuration of electrons

in a set of orbitals with equal (or nearly equal) energy should have as many unpaired electrons spins as possible. This is necessary to obtain the lowest energy due to reduced Coulomb repulsion between spatially dissimilar orbitals. A good example of this is the oxygen molecule, where the ground state is a triplet, *i.e.*, there are two unpaired electrons.

There are several means of including Coulomb correlation on top of the HF method. The most common approaches are based on systematically improving the description of the wave function, *e.g.*, perturbation theory-based methods (*e.g.*, MP2 [46]), coupled cluster methods [*e.g.*, CCSD, CCSD(T)] and multiconfigurational methods (*e.g.*, MCSCF). [47] What all these have in common is the rapidly increasing computational cost. Whereas the cost of the HF method scales as the fourth power of the number of basis functions, $\mathcal{O}(N^4)$*, the simplest correlated method, MP2, already scales as $\mathcal{O}(N^5)$ and CCSD(T) as $\mathcal{O}(N^7)$. But even these methods are still approximations, so clearly a more pragmatic approach should not be dismissed on mere philosophical grounds. Instead, performance, both in speed and accuracy as referenced to the experiment, should be the first and foremost consideration when choosing the method for solving a particular scientific problem.

2.3.1 Density functional theory

Density functional theory (DFT) is a way of including electron correlation at a far lower computational cost than post-HF methods. The basis of DFT was laid by Hohenberg and Kohn in 1964 [49]. They started by considering inhomogeneous electron gas in an external potential $V(\boldsymbol{r})$. Applying the Born-Oppenheimer approximation, a chemical system can be described this way with the Coulomb potential formed by the nuclei as $V(\boldsymbol{r})$. They proved that when the interaction of the electron gas and $V(\boldsymbol{r})$ is written with the help of a universal functional $F_{\mathrm{HK}}[\rho(\boldsymbol{r})]$ independent of $V(\boldsymbol{r})$, the total energy

*This is a formal statement – when using the direct SCF method developed by Almlöf *et al.* [48], the HF method scales $\mathcal{O}(N^2)$ at the limit of infinite system size.

of the system becomes

$$E = \int V(\boldsymbol{r})\rho(\boldsymbol{r})d\boldsymbol{r} + F_{\mathrm{HK}}[\rho(\boldsymbol{r})]. \tag{2.9}$$

Here $\rho(\boldsymbol{r})$ is the electron density at $\boldsymbol{r}$ and E is the ground-state energy of the system corresponding to $V(\boldsymbol{r})$. According to the variational principle, if the energy can be minimized, the corresponding electron density is that of the best approximation for the ground state of the system.

In 1965, Kohn and Sham [50] introduced the Kohn-Sham reference state, a hypothetical non-interacting system of electrons which has the same electron density as the real one. In the K-S reference, the density ρ is exactly the sum of squares of the one-particle states ϕ_i,

$$\rho(\boldsymbol{r}) = \sum_i |\phi_i(\boldsymbol{r})|^2 . \tag{2.10}$$

Next, they divided the functional F_{HK} into three parts: Coulomb repulsion between orbital densities, the kinetic energy of the K-S reference system, and the exchange-correlation potential V_{XC}. The latter describes the interaction between electrons other than the Coulomb repulsion of the averaged charge density, as well as the difference in the kinetic energy between the reference and the real system. There are exact formulas for the first two parts, but the exact form of V_{XC} is unknown. This led to the Kohn-Sham equations, which allow a self-consistent solution of the variational problem in the Hohenberg-Kohn theory, similar to the SCF method used in the wave function formalism,

$$\left(-\frac{1}{2}\boldsymbol{\nabla}^2 + \left[\int \frac{\rho(\boldsymbol{r}_2)}{r_{12}} d\boldsymbol{r}_2 + V_{XC}(\boldsymbol{r}_1) - \sum_K \frac{Z_K}{r_{1K}}\right]\right)\phi_i(\boldsymbol{r}_1) = \epsilon_i\phi_i(\boldsymbol{r}_1). \tag{2.11}$$

Here, K is the nuclear index and Z_K is the charge of nucleus K. The equation is of similar form and purpose as the HF equations (2.6), although we can see a difference between the wave function-based methods and DFT. Whereas in the wave function methods the Hamiltonian is fixed and the description of the wavefunction is systematically improved, in DFT it is the Hamiltonian that becomes effectively changed by changing the exchange-correlation functional.

This also leads to unsystematicity when trying to improve DFT results in a series of calculations, as the connection between changes in V_{XC} and an improvement of the description is seldom clear.

The simplest choice for the functional V_{XC} is the local density approximation (LDA) [51], where the electron density is assumed to only vary slowly, and thus the energy depends on the local electron density similarly as in a homogeneous electron gas, $V_{XC} = V_{XC}[\rho(\boldsymbol{r})]$. LDA was actually formulated by Dirac [52] and Slater [51] before Hohenberg, Kohn and Sham gave DFT its present-day form. The most common version of LDA in modern programs uses Slater's exchange part of the functional with the correlation part formulated by Vosko *et al.* in 1980 [53]. This is known as the Slater-Vosko-Wilk-Nusair (SVWN) functional. As metals can be thought to consist of a gas of mobile electrons (conduction band) in a potential formed by the core electrons and the nuclei, this approximation works fairly well for describing metallic systems, and is still used in solid-state physics. As the electron density in molecular systems can have steep changes, LDA does not work well for them.

Generalized gradient approximation (GGA) functionals [54] were developed to improve the description of systems with non-uniform density. In a GGA functional, the energy depends on the gradient of the density in addition to the density itself, $V_{XC} = V_{XC}[\rho(\boldsymbol{r}), \nabla\rho(\boldsymbol{r})]$.

When the exchange part of a functional is partially replaced by the HF exact exchange, we obtain a hybrid functional [54]. Hybrid functionals are used to improve DFT results by including some of the Fermi correlation intrinsic in HF, which is otherwise difficult to model. As there is no unphysical self-interaction present in HF, unlike pure DFT, hybrid functionals avoid some of it.

In this work mostly GGA functionals are used. Although the basic electronic structure determination can be nearly as fast with hybrid functionals as with GGA functionals when using the appropriate approximations, the magnetic property calculation methods (section 3.2) used could not take

advantage of such speedups. As a result, the computational cost of the property calculation with hybrid functionals can be up to two orders of magnitude higher than with a GGA functional.* Thus, hybrid DFT was only used sparingly, and mostly for comparison purposes, especially so since the results for the systems in Papers I and II were not consistently improved by the hybrid functionals.

2.3.2 Basis sets

Exact representation of the wavefunction in an arbitrary case would require a set of basis functions that is complete. However, such set would be infinite for a real system, and truncations are necessary. The first basis sets historically used were composed of Slater functions, which correctly reproduce the wave function cusp-condition at the nucleus, and also behave asymptotically correctly at large distances [42]. The downside of these functions is that their two-electron integrals are time-consuming to calculate, and consequently computationally easier Gaussian type functions have been mostly used [55]. Gaussian type functions do not behave correctly at either the nucleus or at large distances, so recently Slater functions have regained popularity [56]. In this work, only Gaussian basis functions have been used.

There are several possible goals when constructing or choosing a basis set. Amongst others, basis sets have been constructed to perform well with highly correlated wave function methods [57] (requires inclusion of high angular momentum functions), better reproduction of magnetic properties [58, 59, 60, 61] (the core region is emphasized in the span of Gaussian exponents) or based on the completeness profile [62] of the basis set [63, 64]. The completeness profile acts as a visual aid for estimating the completeness of a basis set.

For this work, the Huzinaga-Kutzelnigg IGLO basis sets [65, 58] (HII, HIII and HIV) were used exclusively for the property calculations on first-

*This depends on the number of nuclei for which the properties are calculated, but as an example of a medium-sized system, the property calculations for $CrCp_2$ in Paper II took 1.25 cpu-h with the PBE functional (GGA), but 90 cpu-h with the PBE0 functional (hybrid).

and second-row main-group atoms, as these had earlier proven to perform well for the calculation of magnetic properties [66]. In Paper III, these were augmented with tight s and p type functions for a better description of spin density at and near the hydrogen nuclei. In Paper IV, diffuse functions were added with the "division-by-three" method.* For the metals, varyingly Faegri's [67] or Munzarová and Kaupp's [59] basis sets were used.

The computational cost of a DFT calculation is mostly determined by the calculation of the Coulomb energy, which formally scales as $\mathcal{O}(N^4)$, where N is the number of basis functions. [54] To speed this up, density fitting methods [68] can be used. These are based on first fitting the density into an auxiliary basis, optimally 2-3 times larger than the original AO basis used for the expansion of MOs [69, 70]. Then the Coulomb energy is rewritten using this fitted density and applying resolution of identity to turn the four-index integrals into three-index integrals. This brings the scaling to $\mathcal{O}(N^3)$ even at the small system limit. The resolution of identity is exactly true only for a complete set of functions, but the error introduced by using it on an incomplete auxiliary basis can be made negligible as compared to errors from an incomplete orbital basis set in the first place. This method is called RI-J DFT [69, 70]. With pre-screening of the integrals to avoid unnecessary calculation of negligible contributions, the scaling can be further reduced to $\mathcal{O}(N^2)$. Advances have also been made with purely AO-based methods that approach linear [$\mathcal{O}(N)$] scaling at the limit of large systems, see, *e.g.*, Ref. [71].

As the use of hybrid functionals requires separate calculation of the HF exchange integrals in addition to the Coulomb integrals, the computational cost is again $\mathcal{O}(N^4)$ to start with, but with the so-called RI-JK approximation [72], similar to that used in RI-J DFT, the cost can be lowered to $\mathcal{O}(N^3)$. Kossmann and Neese [73] have compared the RI-JK approximation with Neese's alternate method [74] for speeding up hybrid functional calculations (RIJCOSX), which is faster than RI-JK for large systems. In Paper

*The smallest exponent in the basis is divided by three and a corresponding primitive function is added to the original basis set.

I, the RI-J approximation was not employed as the Kohn-Sham orbitals were obtained from GAUSSIAN03 [75], which does not include this method. In the other Papers, the RI-J approximation was utilized.

2.3.3 Molecular dynamics

In molecular dynamics (MD), the time development of the nuclear locations is studied by applying Newtonian mechanics on the nuclei in short time steps, usually on the order of 1 fs. The forces are calculated either from a pre-parametrized force field such as Amber [76], or by first-principles electronic structure calculations, in *ab initio* MD (AI-MD) [77]. The initial speeds of the nuclei are usually randomized from the Boltzmann distribution at the desired temperature, optionally the speeds in consequent steps are scaled in order to stabilize the speed distribution before the production phase of the simulation. In this work, AI-MD was used in Paper IV, using RI-DFT with a GGA functional for the electronic structure calculation.

2.3.4 Effective core potentials

The inner core electrons do not contribute to the bonding properties of heavy atoms nearly as much as the valence electrons. To reduce the number of basis functions required for electronic structure calculation, the core electrons and the nucleus can be replaced by an effective core potential (ECP) [78] obtained from an accurate calculation of a single atom. This potential can even include properties not present in a comparable all-electron calculation, if the single-atom calculation is carried out with relativistic methods, as in the Stuttgart group ECPs [79, 80] employed in Papers I and IV.

Chapter 3

Theory

3.1 NMR and ESR spin Hamiltonians

Spin Hamiltonians are effective expressions of energy formed by choosing the experimental variables (such as spin and magnetic field) as the explicit degrees of freedom, commonly in leading order only, and including the measured quantities (such as the shielding tensor $\boldsymbol{\sigma}_K$) as parameters. Implicit degrees of freedom, such as the positions of the nuclei and electrons, are included in the parameters. The NMR spin Hamiltonian for a system of nuclei K with nuclear spins I_K in frequency units is

$$\begin{aligned} H_{\mathrm{NMR}} = &- \frac{1}{2\pi} \sum_K \gamma_K \boldsymbol{I}_K \cdot (\mathbf{1} - \boldsymbol{\sigma}_K) \cdot \boldsymbol{B}_0 \\ &+ \frac{1}{2} \sum_{K \neq L} \boldsymbol{I}_K \cdot (\boldsymbol{D}_{KL} + \boldsymbol{J}_{KL}) \cdot \boldsymbol{I}_L + \sum_K \boldsymbol{I}_K \cdot \boldsymbol{\mathcal{B}}_K \cdot \boldsymbol{I}_K, \end{aligned} \tag{3.1}$$

where γ_K is the gyromagnetic ratio of K, $\boldsymbol{I}_K$ is the nuclear spin, $\boldsymbol{D}_{KL}$ and $\boldsymbol{J}_{KL}$ are the direct and indirect nuclear spin-spin coupling tensors, respectively, and $\boldsymbol{\mathcal{B}}_K$ is the quadrupole coupling tensor.

Magnetic field and spin provide small, time-independent static perturbations to the electronic ground state. Thus, the electronic energy of a system can be written as a Taylor series of these perturbations $\epsilon_1, \epsilon_2, ...$,

$$E(\epsilon_1, \epsilon_2, ...) = E_0 + \sum_n E_n \epsilon_n + \frac{1}{2!} \sum_{m,n} E_{mn} \epsilon_m \epsilon_n + \mathcal{O}(\boldsymbol{\epsilon}^3). \tag{3.2}$$

Here, the coefficients $E_n, E_{mn}, \ldots$ are the derivatives of energy with respect to the perturbations. The values of these derivatives at zero perturbation are magnetic properties:

$$\begin{aligned} E_n &= \left.\frac{\partial E}{\partial \epsilon_n}\right|_{\epsilon_n=0} \\ E_{mn} &= \left.\frac{\partial^2 E}{\partial \epsilon_m \partial \epsilon_n}\right|_{\epsilon_m=0=\epsilon_n} . \end{aligned} \tag{3.3}$$

If $\boldsymbol{I}_K$ and $\boldsymbol{B}_0$ are the perturbations, we obtain the field-independent part of the nuclear shielding tensor as

$$\boldsymbol{\sigma}_K = \frac{1}{\gamma_K} \left.\frac{\partial^2 E(\boldsymbol{I}_K, \boldsymbol{B}_0)}{\partial \boldsymbol{I}_K \partial \boldsymbol{B}_0}\right|_{\boldsymbol{I}_K=\boldsymbol{0}=\boldsymbol{B}_0} . \tag{3.4}$$

In the ESR spin Hamiltonian H^{ESR}, the true electron spin quantum number is replaced by an effective electron spin $\boldsymbol{S}$, defined by requiring $2S+1 =$ number of electron spin states. This introduces an error (assumed to be negligible) when the effective spin and the true spin differ [40], such as when the system has a near degeneracy between a singlet and a triplet state. For a system with effective unpaired electron spin $\boldsymbol{S}$ we have in energy units

$$\begin{aligned} H_{\mathrm{ESR}} = &- \sum_K \gamma_K \boldsymbol{I}_K \cdot (\boldsymbol{1} - \boldsymbol{\sigma}_K^{\mathrm{orb}}) \cdot \boldsymbol{B}_0 + \mu_B \boldsymbol{B}_0 \cdot \boldsymbol{g} \cdot \boldsymbol{S} \\ &+ \sum_K \boldsymbol{S} \cdot \boldsymbol{A}_K \cdot \boldsymbol{I}_K + \boldsymbol{S} \cdot \boldsymbol{D} \cdot \boldsymbol{S}, \end{aligned} \tag{3.5}$$

where $\boldsymbol{g}$ is the electronic g-tensor, $\boldsymbol{A}_K$ is the hyperfine coupling tensor, and $\boldsymbol{D}$ is the zero-field splitting tensor. $\boldsymbol{D}$ is analogous to the sum of $\boldsymbol{\mathcal{B}}$ over the nuclei in the NMR spin Hamiltonian. Choosing as perturbations either the external magnetic field and electron spin, nuclear spin and electron spin, or the second order term in electron spin, we obtain from the ESR spin Hamiltonian

$$\boldsymbol{g} = \frac{1}{\mu_B} \left.\frac{\partial^2 E(\boldsymbol{B}_0, \boldsymbol{S})}{\partial \boldsymbol{B}_0 \partial \boldsymbol{S}}\right|_{\boldsymbol{B}_0=\boldsymbol{0}=\boldsymbol{S}} \tag{3.6}$$

$$\boldsymbol{A}_K = \left.\frac{\partial^2 E(\boldsymbol{I}_K, \boldsymbol{S})}{\partial \boldsymbol{I}_K \partial \boldsymbol{S}}\right|_{\boldsymbol{I}_K=\boldsymbol{0}=\boldsymbol{S}} \tag{3.7}$$

$$\boldsymbol{D} = \left.\frac{\partial^2 E(\boldsymbol{S})}{\partial \boldsymbol{S}^2}\right|_{\boldsymbol{S}=\boldsymbol{0}} . \tag{3.8}$$

3.2 Obtaining magnetic properties from DFT

As described in detail by, *e.g.*, Neese in his 2009 review [81] on the prediction of molecular properties and in Ref. [82], the coupled-perturbed KS (CPKS) scheme is used for obtaining the derivatives required in their DFT calculation. For first-order properties, the perturbed state is not required and the derivatives are acquired simply as

$$\frac{\partial E}{\partial \epsilon_m} = \sum_{\mu\nu} P_{\mu\nu} \left\langle \phi_\mu \left| h_{e_m} \right| \phi_\nu \right\rangle , \tag{3.9}$$

where P is the density matrix.

For second-order properties, the first-order perturbed state is required,

$$\frac{\partial^2 E}{\partial \epsilon_m \partial \epsilon_n} = \sum_{\mu\nu} \left(P_{\mu\nu} \frac{\partial^2 h_{\mu\nu}}{\partial \epsilon_m \partial \epsilon_n} + \frac{\partial P_{\mu\nu}}{\partial \epsilon_m} \frac{\partial h_{\mu\nu}}{\partial \epsilon_n} \right) , \tag{3.10}$$

where the derivative of the density matrix is found by first solving the CPKS equations, for a purely imaginary perturbation these are [82]

$$\begin{pmatrix} M^{\alpha\alpha} & 0 \\ 0 & M^{\beta\beta} \end{pmatrix} \begin{pmatrix} U^{\alpha;\mu} \\ U^{\beta;\mu} \end{pmatrix} = - \begin{pmatrix} V^{\alpha;\mu} \\ V^{\beta;\mu} \end{pmatrix} , \tag{3.11}$$

where

$$\begin{aligned} V_{ia}^{\sigma;\mu} &= \Im \left\langle \phi_i^\sigma \left| h_\mu \right| \phi_a^\sigma \right\rangle \\ M_{ia,jb}^{\sigma\sigma'} &= \left(\epsilon_a^\sigma - \epsilon_i^\sigma \right) \delta_{ia,jb} \delta_{\sigma\sigma'} \\ &\quad + c_{\mathrm{HF}} \delta_{\sigma\sigma'} \left(\left\langle \phi_a^\sigma \phi_j^{\sigma'} \left| r_{12}^{-1} \right| \phi_i^\sigma \phi_b^{\sigma'} \right\rangle - \left\langle \phi_a^\sigma \phi_j^{\sigma'} \left| r_{12}^{-1} \right| \phi_i^\sigma \phi_b^{\sigma'} \right\rangle \right) . \end{aligned} \tag{3.12}$$

Here, c_{HF} is the coefficient denoting the amount of exact exchange in the functional and $\Im$ denotes the imaginary part of the following expression. The solutions U_{ia}^σ are the coefficients when the first-order perturbed orbitals are written as linear combinations of the zeroth-order virtual orbitals,

$$\phi_i^{\sigma(1)} = \sum_a U_{ia}^\sigma \phi_a^{\sigma(0)}, \tag{3.13}$$

and the perturbed density matrix becomes

$$\frac{\partial P_{\mu\nu}}{\partial \epsilon_m} = \sum_{ip} U_{pi}^* c_{\mu p}^* c_{\nu i} + U_{pi} c_{\mu i}^* c_{\nu p} \tag{3.14}$$

Now, it is obvious that the magnetic Hessian M is diagonal for $c_{\mathrm{HF}} = 0$. The solutions are obtained trivially without calculating the $N^2 \times N^2$ two-electron matrix elements (N is the number of basis functions). For a real perturbation, M would be replaced by the electric Hessian, which requires these integrals even for pure functionals. The second-order terms in this work are all purely imaginary, and as such these can be obtained directly when using pure DFT functionals. When using hybrid functionals the matrix equations are too large to be solved directly. Iterative methods are required.

3.3 Breit-Pauli Hamiltonian

The Breit-Pauli (BP) Hamiltonian is a quasirelativistic operator describing a molecular system in the presence of electromagnetic fields. It is obtained by reducing the fully relativistic Dirac-Coulomb-Breit (DCB) Hamiltonian [83] of an electron system into the two-component form with the Foldy-Wouthuysen [84] transformation, and empirically adding nuclear charges, magnetic dipole moments and electric quadrupole moments [40].

The terms of the BP Hamiltonian can be ordered according to increasing even powers in the fine structure constant $\alpha \approx 1/137$, the higher-order terms being decreasingly important due to the rapidly decreasing prefactor. The quantity α^2 appear as an expansion parameter during the Foldy-Wouthuysen transformation of the DCB Hamiltonian into the Pauli Hamiltonian.

For the purposes of this work, the relevant terms of the BP Hamiltonian are those that have a significant effect on the shielding of light atoms in systems containing heavy atoms. This includes those contributing to orbital shielding in the leading order (α^2, *vide infra*, p. 37), and those required to construct hyperfine shielding terms up to order of α^4. For this, terms are needed that contribute to the g-tensor to $\mathcal{O}(\alpha^2)$, hyperfine tensor of light atoms to at most $\mathcal{O}(\alpha^4)$, and zero field splitting in the leading order, $\mathcal{O}(\alpha^4)$. Such terms are also included that can be combined perturbatively to form any of these.

The outlined procedure excludes all terms that are quadratic in the ex-

ternal magnetic field (required, *e.g.*, for the field-dependence of shielding, see Paper II) or nuclear spin (the so-called pseudoquadrupolar terms [85]). Additionally, most of the relativistic two-electron terms are excluded due to their small effect on magnetic properties of light nuclei (in systems containing heavy nuclei) when compared to the corresponding one-electron terms. In the presence of a vector potential $\mathcal{A}$, defined as

$$\boldsymbol{\mathcal{A}} = \boldsymbol{\mathcal{A}}_0 + \boldsymbol{\mathcal{A}}_K, \tag{3.15}$$

where $\boldsymbol{\mathcal{A}}_0$ corresponds to the external homogeneous magnetic field $\boldsymbol{B}_0$ and $\boldsymbol{\mathcal{A}}_K$ corresponds to the field from a point dipole at nucleus K, the considered Hamiltonian becomes

$$\begin{aligned} H^{\mathrm{BP}} \approx\ & H^{\mathrm{KE}} + H^{\mathrm{NE}} + H^{\mathrm{EE}} && (3.16)\\ & + H^{\mathrm{OZ}}_{B_0} && (3.17)\\ & + H^{\mathrm{PSO}}_{K} && (3.18)\\ & + H^{\mathrm{DS}}_{K,B_0} && (3.19)\\ & + H^{\mathrm{SO}} + H^{\mathrm{SS}} && (3.20)\\ & + H^{\mathrm{SZ}}_{B_0} + H^{\mathrm{SZ\text{-}KE}}_{B_0} + H^{\mathrm{SO}}_{B_0} + H^{\mathrm{SO}}_{K} && (3.21)\\ & + H^{\mathrm{FC}}_{K} + H^{\mathrm{SD}}_{K}. && (3.22) \end{aligned}$$

Here, the dependence on nuclear spin or external magnetic field is denoted with K or B_0. Additionally, the terms (3.20 – 3.22) depend linearly on the electron spin, apart from H^{SS}, which is quadratic in it. For the explicit forms of the terms, see Ref. [86].

The first three terms in (3.16 – 3.22) are the kinetic energy and Coulomb attraction/repulsion interactions (NE term being the nucleus-electron attraction and EE the electron-electron repulsion) of the ordinary, unperturbed nonrelativistic Hamiltonian.

The operator H^{DS}_{K,B_0} in (3.19) is the electron nuclear Zeeman coupling term, $H^{\mathrm{OZ}}_{B_0}$ in (3.17) is the orbital Zeeman interaction and H^{PSO}_{K} in (3.18) is the orbital hyperfine interaction. These contributions arise from the coupling of the nuclear spin angular momentum to the orbital angular momenta of

the electrons, and the coupling of the combined angular momentum to the external magnetic field. They can also be described as the interaction of the nuclear magnetic moment with magnetic fields arising from currents induced by the external magnetic field [42].

The operator H^{SO} in (3.20) contains the interaction of electron spin with the orbital angular momenta of electrons, including a single-electron term ($H^{\mathrm{SO(1)}}$) and two-electron terms for both the same electron ($H^{\mathrm{SSO(2)}}$) and other electrons ($H^{\mathrm{SOO(2)}}$). The two-electron terms are computationally expensive to evaluate [87, 88, 89] and therefore these are usually handled with additional approximations, *e.g.*, the atomic mean field (AMFI) method [90, 91], as is also done in this work. The term H^{SS} is the electron-electron spin-spin interaction, including both contact ($H^{\mathrm{SSC(2)}}$) and dipolar ($H^{\mathrm{SSD(2)}}$) terms, of which only the dipolar part is of importance for $\boldsymbol{D}$.

The operator $H_{B_0}^{\mathrm{SZ}}$ in (3.21) is the nonrelativistic spin-Zeeman interaction of the electron spin and the external magnetic field, and $H_{B_0}^{\mathrm{SZ\text{-}KE}}$ is the relativistic "kinetic energy" [86] correction to it. The spin-Zeeman interaction causes the field-induced electron spin polarization in a paramagnetic system, and thus is indirectly responsible for the hyperfine shielding effects handled in this work.

The operator $H_{B_0}^{\mathrm{SO}}$ describes the coupling of the electron spins to the external magnetic field via their orbital angular momenta, it is also known as the gauge-correction term in the context of g-tensor calculations. The term H_K^{SO} is the corresponding coupling of electron spins to the magnetic field of the nuclei. Both $H_{B_0}^{\mathrm{SO}}$ and H_K^{SO} arise from the SO interaction with the magnetic field-dependent part of the generalized momentum

$$\boldsymbol{\pi} = \boldsymbol{p} + \boldsymbol{\mathcal{A}}, \tag{3.23}$$

where $\boldsymbol{\mathcal{A}}$ is the vector potential.

The operator H_K^{FC} in (3.22) is the Fermi contact coupling of electron spins to the nuclear magnetic dipole, in basically just a product of the nuclear spin and the electron spin density at the nucleus [92]. The term H_K^{SD} is the interaction between the nuclear magnetic dipole and the magnetic field of

the electron spins outside the nucleus.

The terms of the BP Hamiltonian used in this work are listed in Table 3.1.

3.3.1 Orbital shielding

The phenomenological basis of NMR shielding is the interaction between the magnetic moment of a nucleus and the magnetic field. The standard theory for the NMR shielding in diamagnetic molecules was laid down by Ramsey in a set of four seminal papers between 1950 and 1952 [93, 94, 95, 96]. There, he defined the shielding in Eq. (1.1) as consisting of the present-day electron nuclear Zeeman $\left\langle H^{\mathrm{DS}}_{K,B_0} \right\rangle$ and orbital hyperfine-orbital Zeeman $\left\langle\left\langle H^{\mathrm{PSO}}_{K}; H^{\mathrm{OZ}}_{B_0} \right\rangle\right\rangle_0$ [†] contributions. They are often called the diamagnetic and paramagnetic shielding terms due to their positive and negative signs, respectively. This terminology is not used in this work to avoid confusion with other meanings of the words,[*] and their sum will subsequently be only referred to as (the leading-order $\mathcal{O}(\alpha^2)$ part of) *orbital* shielding. These two contributions form a gauge-invariant pair, *i.e.*, their individual values depend on the choice of the gauge origin of the vector potential, but their sum remains constant. Thus, neither of them is an observable alone, only the sum can be determined. In calculations, exact gauge invariance is only reached at the limit of a complete basis set.

3.3.2 ESR properties

From Eq. (3.6) we can see that the presentation of the g-tensor in the response theory formalism should include terms linear in both the electron spin and the external magnetic field. In this work, the components of the g-tensor

[†] Linear response notation used [97], $\langle\langle A; B\rangle\rangle_0 = \sum_{m>0} \frac{\langle 0|A|m\rangle\langle m|B|0\rangle + \langle 0|B|m\rangle\langle m|A|0\rangle}{E_0 - E_m}$, where $|m\rangle$ are the excited states and E_m are their energies.

[*] The division to paramagnetic and diamagnetic is in this work used for molecular systems according to whether or not there are unpaired electrons. This should not be confused with the classification of macroscopic substances based on their property to either fortify or weaken the external magnetic field.

Table 3.1: Summary of the terms of the BP Hamiltonian used in this work for property calculations [86].

Term		Properties
H^{SO}	$\frac{1}{4}\alpha^2 g_e \sum_{i,K} \frac{Z_K}{r_{iK}} \boldsymbol{s}_i \cdot \boldsymbol{l}_{iK} - \frac{1}{4}\alpha^2 g_e \sum_{i,j}{}' \boldsymbol{s}_i \cdot \frac{\boldsymbol{l}_{ij}}{r_{ij}^3} - \frac{1}{2}\alpha^2 g_e \sum_{i,j}{}' \boldsymbol{s}_j \cdot \frac{\boldsymbol{l}_{ij}}{r_{ij}^3}$	$\boldsymbol{g}, \boldsymbol{A}^{\mathrm{SO}}, \boldsymbol{D}$
H^{SS}	$\frac{1}{4}\alpha^2 g_e \sum_{i,j}{}' \frac{r_{ij}^2(\boldsymbol{s}_i\cdot\boldsymbol{s}_j)-(\boldsymbol{s}_i\cdot\boldsymbol{r}_{ij})(\boldsymbol{r}_{ij}\cdot\boldsymbol{s}_j)}{r_{ij}^5} - \frac{\pi g_e^2}{3}\alpha^2 \sum_{i,j}{}' \boldsymbol{s}_i \cdot \boldsymbol{s}_j \delta(\boldsymbol{r}_{ij})$	$\boldsymbol{D}$
H_K^{PSO}	$\alpha^2 \gamma_K \sum_i \boldsymbol{I}_K \cdot \frac{\boldsymbol{l}_{iK}}{r_{iK}^3}$	$\boldsymbol{\sigma}, \boldsymbol{A}^{\mathrm{SO}}$
H_K^{SD}	$\frac{1}{2}\alpha^2 g_e \gamma_K \sum_i \boldsymbol{s}_i \cdot \frac{3\boldsymbol{r}_{iK}\boldsymbol{r}_{iK}-\mathbf{1}r_{iK}^2}{r_{iK}^5} \cdot \boldsymbol{I}_K$	$\boldsymbol{A}$
H_K^{FC}	$\frac{4\pi}{3}\alpha^2 g_e \gamma_K \sum_i \delta(\boldsymbol{r}_{iK}) \boldsymbol{s}_i \cdot \boldsymbol{I}_K$	$\boldsymbol{A}$
$H_{B_0}^{\mathrm{OZ}}$	$\frac{1}{2}\sum_i \boldsymbol{l}_{iO} \cdot \boldsymbol{B}_0$	$\boldsymbol{\sigma}$,$\boldsymbol{g}$
$H_{B_0}^{\mathrm{SZ}}$	$\frac{1}{2} g_e \sum_i \boldsymbol{s}_i \cdot \boldsymbol{B}_0$	$\boldsymbol{g}$
$H_{B_0}^{\mathrm{SZ\text{-}KE}}$	$\frac{1}{4}\alpha^2 g_e \sum_i \boldsymbol{S}_i \cdot \boldsymbol{B}_0 \nabla_i^2$	$\boldsymbol{g}$,$\boldsymbol{\sigma}^a$
$H_{B_0}^{\mathrm{SO}}$	$\frac{1}{8}\alpha^2 g_e \sum_N Z_N \sum_i \boldsymbol{s}_i \cdot \frac{\mathbf{1}(\boldsymbol{r}_{iO}\cdot\boldsymbol{r}_{iN})-\boldsymbol{r}_{iO}\boldsymbol{r}_{iN}}{r_{iK}^3} \cdot \boldsymbol{B}_0 - \frac{1}{8}\alpha^2 g_e \sum_{i,j}{}' \boldsymbol{s}_i \cdot \frac{\mathbf{1}(\boldsymbol{r}_{iO}\cdot\boldsymbol{r}_{ij})-\boldsymbol{r}_{iO}\boldsymbol{r}_{ij}}{r_{ij}^3} \cdot \boldsymbol{B}_0$	
	$-\frac{1}{4}\alpha^2 g_e \sum_{i,j}{}' \boldsymbol{s}_j \cdot \frac{\mathbf{1}(\boldsymbol{r}_{iO}\cdot\boldsymbol{r}_{ij})-\boldsymbol{r}_{iO}\boldsymbol{r}_{ij}}{r_{ij}^3} \cdot \boldsymbol{B}_0$	$\boldsymbol{g}$
H_{K,B_0}^{DS}	$\frac{1}{2}\alpha^2 \gamma_K \sum_i \boldsymbol{I}_K \cdot \frac{\mathbf{1}(\boldsymbol{r}_{iO}\cdot\boldsymbol{r}_{iK})-\boldsymbol{r}_{iO}\boldsymbol{r}_{iK}}{r_{iK}^3} \cdot \boldsymbol{B}_0$	$\boldsymbol{\sigma}$

[a] Only in $\mathcal{O}(\alpha^4)$ shielding, not included in this work.

have contributions from

$$g = \left\langle H^{\mathrm{SZ}}_{B_0} \right\rangle + \left\langle H^{\text{SZ-KE}}_{B_0} \right\rangle + \left\langle\left\langle H^{\mathrm{SO}}; H^{\mathrm{OZ}}_{B_0} \right\rangle\right\rangle_0 + \left\langle H^{\mathrm{SO}}_{B_0} \right\rangle . \tag{3.24}$$

The first term is proportional to α^0 and actually reduces to the free electron g-factor $g_e\mathbf{1}$, the rest are proportional to α^2. In most cases, the g-tensor symmetrized as $\sqrt{\boldsymbol{g}^T\boldsymbol{g}}$ is used instead of the full, usually* nonsymmetric g-tensor, and this has also been done throughout the present work.

Likewise, we see from (3.7) that the presentation of hyperfine coupling should include terms linear in both electron spin and nuclear spin. These include [40, 98]

$$A_K = \left\langle H^{\mathrm{FC}}_K \right\rangle + \left\langle H^{\mathrm{SD}}_K \right\rangle + \left\langle\left\langle H^{\mathrm{PSO}}_K; H^{\mathrm{SO}} \right\rangle\right\rangle_0 + \left\langle H^{\mathrm{SO(1)}}_K \right\rangle , \tag{3.25}$$

where the last two terms are the spin-orbit (SO) contributions.

The SO terms were first implemented as *a posteriori* corrections in first-principles calculations by Belanzoni *et al.* in 1995 [99]. The first implementation of the SO terms $\left\langle H^{\mathrm{SO(1)}}_K \right\rangle$ and $\left\langle\left\langle H^{\mathrm{PSO}}_K; H^{\mathrm{SO}} \right\rangle\right\rangle_0$ for the $\boldsymbol{A}$ tensor of light nuclei allowing for spin polarization in the unrestricted KS framework was by Arbuznikov *et al.* in 2004 [100]. In Paper I, the implementation of Ref. [100] was used, but the terms including $\left\langle H^{\mathrm{SO(1)}}_K \right\rangle$ were omitted because their calculation would have required information about the integration grid, which could not be conveyed in the interfacing process between the two computer programs used. In the other three papers, the $\left\langle H^{\mathrm{SO}}_K \right\rangle$ term was not implemented in the property code at all. In the usual approximation of point-like nuclear magnetic dipole, the $\left\langle H^{\mathrm{SO}}_K \right\rangle$ terms have the problem that the integrals are not defined for terms with the same nucleus both in the SO-operator and the PSO-operator. The omission of the operator is not expected to create a large error in this work, as the $\left\langle H^{\mathrm{SO}}_K \right\rangle$ terms are important only for the heavy nuclei.

In its general formulation [40], the zero-field splitting (ZFS) tensor consists of spin-spin contributions, $\left\langle H^{\mathrm{SS}} \right\rangle$, and second-order spin-orbit contributions, $\left\langle\left\langle H^{\mathrm{SO}}; H^{\mathrm{SO}} \right\rangle\right\rangle_0$. This formulation, as implemented in the ORCA

*Depending on the symmetry of the molecule.

program [101, 102], is used for all the ZFS tensors in Papers II and III. It is noteworthy that in a genuinely relativistic approach, SO effects would be naturally included in the ground state wave function. The g and $\boldsymbol{A}$ tensors then become explicitly first-order properties, and as such would not require a coupled perturbed treatment when using a variational electronic structure method.

3.4 Hyperfine shielding theory before present work

The hyperfine shielding in paramagnetic molecules is caused by the interaction of the nuclei with the electron cloud, which has been spin-polarized by the external magnetic field. While Ramsey's theory also applies to orbital shielding in paramagnetic molecules [18], the magnetic moment of an electron is two to three orders of magnitude larger than that of nuclei. Thus, the electron spin couples to the nuclear spins much stronger than the other nuclei, which induce only a small change in resonance frequencies via spin-spin coupling. The electrons can also move close to the nuclei, with non-zero electron densities even at their exact locations [42]. In a diamagnetic molecule, the effects from the two electrons with paired spins in each spatial orbital closely cancel each other. Then, only contributions arising from triplet excitations such as within nuclear spin-spin coupling [8, 9] and spin-orbit (SO) corrections to Ramsey's orbital shielding [103], are non-zero.

The first hyperfine effect in pNMR to be theoretically described was the Fermi contact shielding, the direct coupling of the nuclear spin to the electron spin density at the nuclear position. McConnell formulated it in 1958 [11] as

$$\boldsymbol{\sigma}_{\mathrm{con}} = -\frac{\pi}{\gamma}\frac{S(S+1)}{3kT} g_{\mathrm{iso}} A_{\mathrm{con}} \mathbf{1}, \tag{3.26}$$

where k is the Boltzmann constant, T is temperature, S is the electron spin quantum number of the system, γ is the nuclear gyromagnetic ratio (in MHz/T), g_{iso} is the isotropic electron g-value and A_{con} is the isotropic

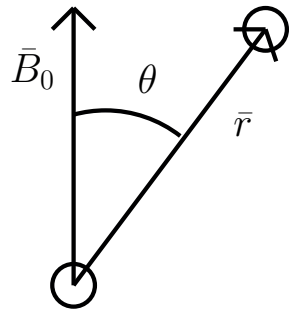

Figure 3.1: Geometry parameters in Kurland and McGarvey's pseudocontact shift. The vector $\boldsymbol{r}$ is defined as pointing from the electron spin (usually the paramagnetic metal center) to the NMR nucleus.

hyperfine Fermi contact coupling constant (in Hz). In this theory, the pseudocontact (PC) shielding is defined as contribution to the isotropic σ due to the hyperfine pseudocontact coupling constant, $A_{\mathrm{PC}} = A - A_{\mathrm{con}}$ [12]. He defined the spin-dipole part of the shielding tensor, caused by the coupling of the magnetic dipole of the nucleus to the magnetic field of the unpaired electrons outside of the nucleus. The dipolar part of shielding tensor was defined as

$$\sigma_{\epsilon\tau}^{\mathrm{dip}} = -\frac{\pi}{\gamma}\frac{S(S+1)}{3kT} g_{\mathrm{iso}} A_{\epsilon\tau}^{\mathrm{dip}}, \tag{3.27}$$

where the $A_{\epsilon\tau}^{\mathrm{dip}}$ terms are the components of the dipolar hyperfine coupling tensor (here in Hz), defined in atomic units as

$$A_{K,\epsilon\tau}^{\mathrm{dip}} = \frac{1}{2}\alpha^2 g_e \gamma_K \sum_i \left\langle 0 \left| \frac{3 r_{iK,\epsilon} r_{iK,\tau} - \delta_{\epsilon\tau} r_{iK}^2}{r_{iK}^5} \right| 0 \right\rangle. \tag{3.28}$$

These old versions of the shielding formulas are correct for the $S = 1/2$ case, but they should be compared with the more general theory in Section 3.5. In McConnell's theory, the Fermi contact shift is purely isotropic, and the dipolar part is purely anisotropic, while in the present work they are generally sums of different tensorial ranks due to zero-field splitting effects for $S > 1/2$.

In 1970, Kurland and McGarvey [104] defined the isotropic PC shielding as resulting from the dipolar interaction between the electronic spin polariza-

tion and the magnetic moment of a nucleus at a distance where the electron spin density is negligible. Starting from the parallel ($\chi_\parallel$) and transverse ($\chi_\perp$) magnetic susceptibilities in a cylindrically symmetric case, they derived an empirical formula where this part of shielding in paramagnetic molecules mainly depends on the location of the NMR nucleus relative to a paramagnetic metal centre as

$$\sigma_{\mathrm{PC}}(B_0) = (\chi_\parallel - \chi_\perp)\frac{1-3\cos^2\theta}{12\pi r^3}\left(1+\frac{B_0^2}{6\mu_0 kT}\right). \tag{3.29}$$

In this equation, r is the distance between the NMR nucleus and the metal centre, μ_0 is the vacuum permeability, and θ is the angle between the direction of the spin magnetization of the centre (direction of $\boldsymbol{B}_0$) and the direction of the NMR nucleus from the location of the assumed point-like electron spin distribution, see Fig. 3.1. The two terms (last set of parenthesis) are the field-independent and leading-order field-dependent parts. There is no first-order (in B_0) term because shielding is invariant in time reversal and $\boldsymbol{B}$ is time-odd. This formula gives a simple geometric relation between the magnitude of the pseudocontact shift of different nuclei in a paramagnetic system and their locations with respect to the (often) metal centre housing the electron spin. PC-shift isosurfaces are for this reason often used in empirical NMR spectroscopy of, *e.g.*, metalloproteins [5]. Generally, in experimental work the decomposition of the shift is performed as

$$\delta_{\mathrm{exp}} = \delta_{\mathrm{con}} + \delta_{\mathrm{PC}} + \delta_{\mathrm{orb}}, \tag{3.30}$$

where the orbital shift term δ_{orb} includes the comparison to a diamagnetic reference compound as per Eq. (1.2). Kurland and McGarvey's formula still dominates the field also in computational determination of the hyperfine shielding, along with the idea that the orbital shielding a nucleus in a paramagnetic compound is approximately equal to that experimentally measured in a "corresponding"* diamagnetic compound [105].

*For metal complexes this is a closed-shell system, where either the central ion is in a different oxidation state, or it has been replaced by an element near it in the periodic table to produce an isoelectronic orbital structure. For example, a possible diamagnetic analogue for $CoCp_2$ would be $FeCp_2$.

The next refinement of the McConnell theory was made by Rinkevicius *et al.* in 2003 [18], when they formulated a systematic leading-order nonrelativistic theory for the shielding in paramagnetic molecules, which includes Ramsey's orbital shielding for the paramagnetic system proper, and McConnell's $\boldsymbol{\sigma}_{\mathrm{con}}$ and $\boldsymbol{\sigma}_{\mathrm{dip}}$ terms. This work was the first one to use the response theory formulation [97] for hyperfine shieldings.

In 2004, Moon and Patchkovskii [10] published a general theory of paramagnetic shielding for doublet ($S = \frac{1}{2}$) systems, which for the first time introduced the present notation leading to a scalar product of ESR $\boldsymbol{g}$ and $\boldsymbol{A}$ tensors. They replaced the free-electron g factor g_e by the g-tensor, giving rise to four new corrections to the leading-order contributions, $\Delta g_{\mathrm{iso}} A_{\mathrm{con}}$, $\Delta\tilde{\boldsymbol{g}} A_{\mathrm{con}}$, $\Delta g_{\mathrm{iso}} \boldsymbol{A}_{\mathrm{dip}}$ and $\Delta\tilde{\boldsymbol{g}} \boldsymbol{A}_{\mathrm{dip}}$, where $\Delta\boldsymbol{g}$ is the g-shift tensor, the difference between the full g-tensor and the isotropic free electron g-tensor. The quantities Δg_{iso} and $\Delta\tilde{\boldsymbol{g}}$ are the isotropic and anisotropic parts, respectively. These are defined as

$$\Delta\boldsymbol{g} = \boldsymbol{g} - g_e\mathbf{1} \tag{3.31}$$

$$\Delta g_{\mathrm{iso}} = \mathrm{Tr}(\Delta\boldsymbol{g})/3 \tag{3.32}$$

$$\Delta\tilde{\boldsymbol{g}} = \Delta\boldsymbol{g} - \Delta g_{\mathrm{iso}}\mathbf{1}. \tag{3.33}$$

The second new contribution ($\Delta\tilde{\boldsymbol{g}} A_{\mathrm{con}}$) adds an anisotropic part to the Fermi contact shielding and the fourth ($\Delta\tilde{\boldsymbol{g}} \boldsymbol{A}_{\mathrm{dip}}$) adds an isotropic part to dipolar shielding. This last term corresponds to the geometry-dependent definition of the pseudocontact shielding. When this thesis work was started, the formulation of Moon and Patchkovskii was the latest advancement in the field.

3.5 General theory of nuclear shielding for arbitrary spin state

In the formulation of Moon and Patchkovskii [10] for the Cartesian $\epsilon\tau$ component of the nuclear shielding tensor $\boldsymbol{\sigma}$ of nucleus K, the shielding term in the NMR spin Hamiltonian is defined via the Boltzmann average of energy

terms bilinear in $\boldsymbol{B}_0$ and $\boldsymbol{I}_K$,

$$\langle E\left(\boldsymbol{B}_0, \boldsymbol{I}_K\right)\rangle = \frac{\sum_n E_n(\boldsymbol{B}_0, \boldsymbol{I}_K) e^{-W_n(\boldsymbol{B}_0, \boldsymbol{I}_K)/kT}}{\sum_n e^{-W_n(\boldsymbol{B}_0, \boldsymbol{I}_K)/kT}}. \tag{3.34}$$

Here, the states n include the ground-state multiplet as well as low-lying excited electronic states. The energies W_n are associated with the electronic state manifold and the energies E_n with the nuclear spin Zeeman energetics. They are separated for bookkeeping purposes so that the slightly different approximations for the two can be employed consistently.

The expectation value $E_n = \langle n\,|E|\,n\rangle$ is expanded in a power series of $\boldsymbol{B}_0$ and $\boldsymbol{I}_K$,

$$\begin{aligned} E_n(\boldsymbol{B}_0, \boldsymbol{I}_K) = E_n^{(0,0)} &+ \sum_\mu E_n^{(\mu,0)} B_{0,\mu} + \sum_\tau E_n^{(0,\tau)} I_{K,\tau} \\ &+ \sum_{\mu\tau} E_n^{(\mu,\tau)} B_{0,\mu} I_{K,\tau} + \frac{1}{2}\sum_{\mu\nu} E_n^{(\mu\nu,0)} B_{0,\mu} B_{0,\nu} \\ &+ \frac{1}{2}\sum_{\mu\nu\tau} E_n^{(\mu\nu,\tau)} B_{0,\mu} B_{0,\nu} I_{K,\tau} + \ldots \end{aligned} \tag{3.35}$$

$$E_n^{(\mu\nu\ldots,\tau)} = \left(\frac{\partial^m E_n}{\partial B_{0,\mu}\partial B_{0,\nu}\ldots\partial I_{K,\tau}}\right)_{\boldsymbol{B}_0=\boldsymbol{0}=\boldsymbol{I}_K}, \tag{3.36}$$

where m is the total number of differentiations. Only terms up to linear in $\boldsymbol{I}_K$ are shown, because the shielding term in the spin Hamiltonian depends linearly on the nuclear spin in the present formulation. For W_n, a similar expression can be written, and simplified by approximating that the transitions between the nuclear spin Zeeman states are much slower than those between the electronic states. The electronic states can be thought to form an equilibrium manifold with an averaged Curie spin. The interaction of the nuclei with this averaged spin affects the energy levels between which the nuclear spin Zeeman transitions take place. Thus, we can omit the terms including $\boldsymbol{I}_K$ from the expression for W_n,

$$\begin{aligned} W_n(\boldsymbol{B}_0, \boldsymbol{I}_K) \approx W_n(\boldsymbol{B}_0, \boldsymbol{0}) = W_n^{(0,0)} &+ \sum_\mu E_n^{(\mu,0)} B_{0,\mu} \\ &+ \frac{1}{2}\sum_{\mu\nu} E_n^{(\mu\nu,0)} B_{0,\mu} B_{0,\nu} + \ldots \end{aligned} \tag{3.37}$$

In Moon and Patchkovskii's work [10] the shielding tensor $\boldsymbol{\sigma}$ was for the $S = \frac{1}{2}$ case defined as a derivative of the expectation value on the left-hand-side (LHS) of Eq. 3.34 [see Eq. (20.14) in Ref. [10]],

$$\boldsymbol{\sigma}_K = \frac{1}{\gamma_K} \frac{\partial^2 \langle E\left(\boldsymbol{B}_0, \boldsymbol{I}_K\right)\rangle}{\partial \boldsymbol{I}_K \partial \boldsymbol{B}_0}, \tag{3.38}$$

which works if the energies of the spin Zeeman states have linear dependence on the magnetic field consistent with the shielding being independent of the magnetic field. However, the actual observed $m_s \neq 0$ energy states in the $S > 1/2$ case have a nonlinear dependence on the field, and thus if direct derivation is used for the general case, it leads to unphysical complex values for shielding. Therefore, our formulation as introduced in paper II defines the LHS of Eq 3.34 as

$$\langle E\left(\boldsymbol{B}_0, \boldsymbol{I}_K\right)\rangle = \gamma_K \sum_{\epsilon\tau} B_{0,\epsilon} \sigma_{\epsilon\tau} I_{K,\tau}. \tag{3.39}$$

When Eq. (3.34) is multiplied by the partition function, we obtain

$$\begin{aligned} &\gamma \sum_{\epsilon\tau} B_{0,\epsilon} \sigma_{\epsilon\tau} I_{K,\tau} \sum_n e^{-W_n(\boldsymbol{B}_0,\boldsymbol{0})/kT} \\ &\quad = \sum_n E_n(\boldsymbol{B}_0, \boldsymbol{I}_K) e^{-W_n(\boldsymbol{B}_0,\boldsymbol{0})/kT}. \end{aligned} \tag{3.40}$$

The field-independent leading-order term of $W_n(\boldsymbol{B}_0, \boldsymbol{0})$ is much larger than the rest, so we can approximate

$$\begin{aligned} &e^{-W_n(\boldsymbol{B}_0,\boldsymbol{0})/kT} \\ &\approx e^{-W_n^{(0,0)}/kT} \left\{ 1 - \frac{1}{kT} \left[\sum_\mu W_n^{(\mu,0)} B_{0,\mu} + \frac{1}{2} \sum_{\mu\nu} W_n^{(\mu\nu,0)} B_{0,\mu} B_{0,\nu} + \ldots \right] \right. \\ &\left. + \frac{1}{2(kT)^2} \left[\sum_\mu W_n^{(\mu,0)} B_{0,\mu} + \ldots \right]^2 - \ldots \right\}. \end{aligned} \tag{3.41}$$

Next, $\sigma_{\epsilon\tau}$ is also written as a power series in $\boldsymbol{B}_0$ to separate the field-independent part of the shielding from the field-dependent part,

$$\sigma_{\epsilon\tau} = \sigma_{\epsilon\tau}^{(0)} + \frac{1}{3!} \sum_{\mu\nu} \sigma_{\epsilon\tau\mu\nu}^{(2)} B_{0,\mu} B_{0,\nu} + \ldots, \tag{3.42}$$

where only even powers appear, as justified on p. 29. It should be noted that the prefactor of the leading-order field-dependent part is 1/3! because the shielding term in the NMR spin Hamiltonian depends linearly on B_0, which brings the corresponding terms in the series expansion up by one step.

We can group the terms obtained by inserting the approximate expansions of (3.41) and (3.42) into (3.40). Using the shorthand $P_n(0) = e^{-W_n^{(0,0)}/kT}$ we obtain

$$\begin{aligned}
&\gamma_K \sum_{n\epsilon\tau} P_n(0) \Bigg[B_{0,\epsilon}\sigma_{\epsilon\tau}^{(0)} I_{K,\tau} \\
&\quad -\frac{1}{2}\frac{1}{kT}\sum_{\mu\nu} W_n^{(\mu\nu,0)} B_{0,\mu}B_{0,\nu}B_{0,\epsilon}\sigma_{\epsilon\tau}^{(2)} I_{K,\tau} + \ldots \Bigg] \\
&= \sum_n E_n(\boldsymbol{B}_0, \boldsymbol{I}_K) P_n(0) \Bigg[1 - \frac{1}{kT}\sum_{\mu} W_n^{(\mu,0)} B_{0,\nu} \\
&\quad -\frac{1}{2}\frac{1}{kT}\sum_{\mu\nu} W_n^{(\mu\nu,0)} B_{0,\mu}B_{0,\mu} + \ldots \Bigg],
\end{aligned} \tag{3.43}$$

where $\sigma_{\epsilon\tau}^{(n)}$ are the $\epsilon\tau$ components of the coefficients in (3.42), in terms that depend on $\boldsymbol{B}_0^n$. Now, we can apply the expansion in (3.35) to obtain for the right-hand side of (3.43):

$$\begin{aligned}
\mathrm{RHS} = \sum_n P_n(0) \Bigg[& E_n^{(0,0)} + \sum_\mu E_n^{(\mu,0)} B_{0,\mu} \\
& + \sum_\rho E_n^{(0,\rho)} I_{K,\rho} + \sum_{\mu\rho} E_n^{(\mu,\rho)} B_{0,\mu} I_{K,\rho} \\
& - \frac{1}{kT}\sum_\epsilon W_n^{(\epsilon,0)} E_n^{(0,0)} B_{0,\epsilon} - \frac{1}{kT}\sum_{\epsilon\mu} W_n^{(\epsilon,0)} E_n^{(\mu,0)} B_{0,\mu} B_{0,\epsilon} \\
& - \frac{1}{kT}\sum_{\epsilon\rho} W_n^{(\epsilon,0)} E_n^{(0,\rho)} I_{K,\rho} B_{0,\epsilon} - \frac{1}{kT}\sum_{\epsilon\mu\rho} W_n^{(\epsilon,0)} E_n^{(\mu,\rho)} B_{0,\mu} I_{K,\rho} B_{0,\epsilon} + \ldots \Bigg],
\end{aligned} \tag{3.44}$$

and equate the powers in B_0 on both sides of the equation. Then, similarly to Ref. [10], we can make use of the requirement of time-reversal symmetry of the observable shielding to remove the time-odd terms, *i.e.*, those with

Boltzmann averages of terms that have an odd number of derivations wrt. $\boldsymbol{B}_0$ and/or $\boldsymbol{I}_K$. The leading-order part can be be identified with the field-independent part of shielding in (3.42),

$$\sigma_{\epsilon\tau}^{(0)} = \frac{1}{\gamma}\left\langle E^{(\epsilon,\tau)}\right\rangle_0 - \frac{1}{\gamma kT}\left\langle W^{(\epsilon,0)}E^{(0,\tau)}\right\rangle_0, \tag{3.45}$$

where the Boltzmann averages at the limit of zero magnetic field are in shorthand

$$\langle O\rangle_0 = \frac{\sum_n \langle n\,|O|\,n\rangle\, e^{-W_n^{(0,0)}/kT}}{\sum_n e^{-W_n^{(0,0)}/kT}} = \frac{\sum_n O_n P_n(0)}{\sum_n P_n(0)}. \tag{3.46}$$

The energy derivatives in the expression for the shielding tensor can be obtained from the ESR spin Hamiltonian, (3.5), used here as the effective energy expression

$$W^{(\epsilon,\tau)} = H_{\mathrm{ESR}}^{(\epsilon,\tau)} = \gamma\sigma_{\epsilon\tau}^{\mathrm{orb}} \tag{3.47}$$

$$W^{(\epsilon,0)} = H_{\mathrm{ESR}}^{(\epsilon,0)} = \mu_B \sum_a g_{\epsilon a} S_a \tag{3.48}$$

$$E^{(0,\tau)} = H_{\mathrm{ESR}}^{(0,\tau)} = \sum_b A_{b\tau} S_b. \tag{3.49}$$

Hence, the temperature-independent part can be identified as Ramsey's orbital shielding, whereas the temperature-dependent part becomes

$$-\frac{1}{\gamma kT}\left\langle E^{(\epsilon,0)}E^{(0,\tau)}\right\rangle_0 = -\frac{\mu_B}{\gamma kT}\sum_{ab} g_{\epsilon a}A_{b\tau}\left\langle S_a S_b\right\rangle_0, \tag{3.50}$$

which depends on the ESR g and $\boldsymbol{A}$ tensors as well as the expectation value of the dyadic of the effective electron spin operator with itself. This expectation value should in the general case be taken in the manifold of zero-field split states (*vide infra*).

In an $S = 1/2$ system, the electronic states are degenerate at the limit of zero magnetic field, *i.e.*, there is no zero-field splitting, and this becomes simply the product $\langle S_a S_b\rangle_0 = S^2\delta_{ab}/3 = S(S+1)\delta_{ab}/3$ as in the formalisms of both Rinkevicius *et al.* [18] and Moon and Patchkovskii [10]. This step was also taken in Paper I.

Looking at the next order in B_0 of (3.43), we can write the leading-order field-dependent shielding as

$$\begin{aligned}\sigma^{(2)}_{\epsilon\mu\nu\tau} = \frac{1}{\gamma}\frac{1}{3!}P_{\epsilon\mu\nu}\Bigg\{ & \left\langle E^{\epsilon\mu\nu,\tau}\right\rangle_0 \\ & -\frac{1}{kT}\Bigg[\left\langle W^{(\epsilon\mu\nu,0)}E^{(0.\tau)}\right\rangle_0 + 3\left\langle W^{(\epsilon\mu,0)}E^{(\nu,\tau)}\right\rangle_0 \\ & +3\left\langle W^{(\epsilon,0)}E^{(\mu\nu,\tau)}\right\rangle_0 + \frac{1}{2}\gamma\sigma^{(0)}_{\epsilon\tau}\left\langle W^{(\mu\nu,0)}\right\rangle_0\Bigg] \\ & +\frac{1}{(kT)^2}\Bigg[3\left\langle W^{(\epsilon,0)}W^{(\mu\nu,0)}E^{(0,\tau)}\right\rangle_0 + 3\left\langle W^{(\epsilon,0)}W^{(\mu,0)}E^{(\nu,\tau)}\right\rangle_0 \\ & +\frac{1}{2}\gamma\sigma^{(0)}_{\epsilon\tau}\left\langle W^{(\mu,0)}W^{(\nu,0)}\right\rangle_0\Bigg] \\ & -\frac{1}{(kT)^3}\left\langle W^{(\epsilon,0)}W^{(\mu,0)}W^{(\nu,0)}E^{(0,\tau)}\right\rangle_0\Bigg\},\end{aligned} \tag{3.51}$$

where $P_{\epsilon\mu\nu}$ denotes the sum over all 6 permutations of the indices $\epsilon\mu\nu$. The new derivatives compared to the field-independent case are:

- $E^{(\epsilon\gamma\delta,\tau)}$, the B_0^2 dependence of $\boldsymbol{\sigma}_{\text{orb}}$
- $E^{(\epsilon\gamma,\tau)}$, the B_0^2 dependence of $\boldsymbol{A}$
- $W^{(\epsilon\gamma\delta,0)}$, the B_0^2 dependence of $\boldsymbol{g}$
- $W^{(\gamma\delta,0)}$, magnetizability

Of these, there are existing computational tools for the field dependence of orbital shielding (for diamagnetic systems) [106, 107] and the magnetizability, which at the zero-field limit is a standard molecular property, but in a finite field has not been studied much [108, 109]. Additionally, $\sigma^{(2)}$ depends on the field-independent $\sigma^{(0)}$.

In the $S > \frac{1}{2}$ case, the states $|n\rangle$ over which the expectation value should be taken as eigenfunctions of $H_{\text{ZFS}} = \boldsymbol{S}\cdot\boldsymbol{D}\cdot\boldsymbol{S}$. This is obtained from the ESR spin Hamiltonian by setting the magnetic field and the nuclear spin to zero, in accordance with (3.46), and their energies as the eigenvalues $W_n^{(0,0)}$.

A natural choice for the diagonalization of $\boldsymbol{S} \cdot \boldsymbol{D} \cdot \boldsymbol{S}$ is to express the zero-field-split states $|n\rangle$ in terms of the eigenstates $|m_S\rangle$ of S_z, as

$$\langle n \left| S_a S_b \right| n \rangle = \sum_{m_S, m'_S} C_n^{m'_S *} C_n^{m_S} \left\langle m'_S \left| S_a S_b \right| m_S \right\rangle , \tag{3.52}$$

where the matrix elements $\langle m'_S \left| S_a S_b \right| m_S \rangle$ dependend only on the total spin of the system.

The above described formulation for paramagnetic shielding, introduced in Paper II, is rigorous and applicable for the ground state of any open-shell system, unlike any preceding formulation, which were limited either to the doublet state such as that in Paper I and Ref. [10] or by symmetry as in Ref. [25]. Furthermore, in contrast to the present work, Hrobárik *et al.* [25] formulated the zero-field splitting effects as *a posteriori* corrections, and as such the formulation was not equally rigorous. At the level applied in Papers II and III, the present formulation only gives the shielding at the $B_0 = 0$ limit, but if the terms in (3.51) are implemented, the leading-order magnetic field dependence will be correctly included.

Thermally excited electronic states of different spin multiplicity from the ground state can be handled by adding these to the Boltzmann sum in (3.34), so that the total shielding is the sum of the shieldings in the individual states multiplied by their normalized Boltzmann weights.

3.5.1 Analysis of hyperfine shielding

To determine the paramagnetic shielding as per Eqs. (3.45) and (3.50), any suitable quantum-chemical implementation of $\boldsymbol{\sigma}_{\mathrm{orb}}$, $\boldsymbol{g}$, $\boldsymbol{A}$ and $\boldsymbol{D}$ can be used. Preferably these should be obtained at a consistent level of theory. In Paper I, the following break-downs were employed for $\boldsymbol{g}$ and $\boldsymbol{A}$ (with orders in the

fine structure constant marked below the terms),

$$\boldsymbol{g} = \underset{\alpha^0}{(g_e} + \underset{\alpha^2}{\Delta g_{\mathrm{iso}})\mathbf{1}} + \underset{\alpha^2}{\Delta\tilde{\boldsymbol{g}}} \tag{3.53}$$

$$\boldsymbol{A} = A_{\mathrm{con}}\mathbf{1} + \boldsymbol{A}_{\mathrm{dip}} + \boldsymbol{A}_{\mathrm{SO}} \tag{3.54}$$

$$= \underset{\alpha^2}{(A_{\mathrm{con}}} + \underset{\alpha^4}{A_{\mathrm{PC}})\mathbf{1}} + \underset{\alpha^2}{\boldsymbol{A}_{\mathrm{dip}}} + \underset{\alpha^4}{\boldsymbol{A}_{\mathrm{dip,2}}} + \underset{\alpha^4}{\boldsymbol{A}_{\mathrm{as}}} \tag{3.55}$$

where Δg_{iso} and $\Delta\tilde{\boldsymbol{g}}$ are the isotropic and anisotropic parts of the terms of $\Delta\boldsymbol{g}$, see p. 30.

The further breakdown of $\boldsymbol{A}_{\mathrm{SO}}$ is defined in accordance with Eqs. (A.1 – A.2) in Appendix A. As before, A_{con} is the isotropic Fermi contact part of hyperfine coupling, A_{PC} is the isotropic spin-orbit term, $\boldsymbol{A}_{\mathrm{dip}}$ is the nonrelativistic anisotropic spin-dipole part, and $\boldsymbol{A}_{\mathrm{dip,2}}$ is now its symmetric spin-orbit counterpart, and $\boldsymbol{A}_{\mathrm{as}}$ is the remaining, antisymmetric anisotropic part of $\boldsymbol{A}_{\mathrm{SO}}$, which has no nonrelativistic counterpart. The $\boldsymbol{A}_{\mathrm{SO}}$ terms were for the first time introduced in shielding calculations in Paper I. In the present thesis, the hyperfine shielding terms were included up to α^4, which means in practice including the g-tensor up to α^2 and $\boldsymbol{A}$ tensor up to α^4 excluding, however, the combinations of the terms that would lead to α^6 contributions. The orbital shielding, on the other hand, was included (somewhat inconsistently) only up to α^2 because there currently is no computational implementation available that includes the higher-order terms in open-shell systems. In the paramagnetic case, the hyperfine shielding terms are so large that the α^4 orbital shielding terms would be small in comparison, especially for the light nuclei, which are the primary target of pNMR studies [5].

When only the combinations up to α^4 are included, there are nine terms for the hyperfine shielding, as seen in Table 3.2. In the $S = \frac{1}{2}$ case, as described in Papers I and IV, only terms 1, 3, 6 and 9 contribute to the isotropic shielding constant. When the zero-field splitting is included for higher spin multiplicities, as in Papers II and III, all the terms except the naturally anisotropic term 5 have an isotropic part, the dominating new contribution being the $\mathcal{O}(\alpha^2)$ dipolar term 2.

The terms can be grouped according to either their phenomenological

Table 3.2: Order in the fine structure constant α and tensorial ranks of the hyperfine shielding terms in paramagnetic substances in both doublet and higher-multiplicity spin states.

				Tensorial rank[a]	
Number	Term in $\sigma_{\epsilon\tau}$	Symbol	Order	$S = 1/2$	$S > 1/2$
	σ_{orb}	orb	$\mathcal{O}(\alpha^2)$	0,2,1	0,2,1
1	$g_e A_{\mathrm{con}} \langle S_\epsilon S_\tau \rangle_0$	con	$\mathcal{O}(\alpha^2)$	0	0,2
2	$g_e \Sigma_b A^{\mathrm{dip}}_{b\tau} \langle S_\epsilon S_b \rangle_0$	dip	$\mathcal{O}(\alpha^2)$	2	0,2,1
3	$g_e A_{\mathrm{PC}} \langle S_\epsilon S_\tau \rangle_0$	con,2	$\mathcal{O}(\alpha^4)$	0	0,2
4	$g_e \Sigma_b A^{\mathrm{dip,2}}_{b\tau} \langle S_\epsilon S_b \rangle_0$	dip,2	$\mathcal{O}(\alpha^4)$	2	0,2,1
5	$g_e \Sigma_b A^{\mathrm{as}}_{b\tau} \langle S_\epsilon S_b \rangle_0$	as	$\mathcal{O}(\alpha^4)$	1	2,1
6	$\Delta g_{\mathrm{iso}} A_{\mathrm{con}} \langle S_\epsilon S_\tau \rangle_0$	con,3	$\mathcal{O}(\alpha^4)$	0	0,2
7	$\Delta g_{\mathrm{iso}} \Sigma_b A^{\mathrm{dip}}_{b\tau} \langle S_\epsilon S_b \rangle_0$	dip,3	$\mathcal{O}(\alpha^4)$	2	0,2,1
8	$A_{\mathrm{con}} \Sigma_a \Delta\tilde{g}_{\epsilon a} \langle S_a S_\tau \rangle_0$	con,aniso	$\mathcal{O}(\alpha^4)$	2,1	0,2,1
9	$\Sigma_{ab} \Delta\tilde{g}_{\epsilon a} A^{\mathrm{dip}}_{b\tau} \langle S_a S_b \rangle_0$	pc	$\mathcal{O}(\alpha^4)$	0,2,1	0,2,1

[a]Rank-0, 2, and 1 contributions correspond to the isotropic shielding constant and anisotropic symmetric as well as antisymmetric terms, respectively.

origin or interpretation of measurements. In their review of computational pNMR spectroscopy, Kaupp and Köhler [110] labelled terms 1, 3 and 6 together as the contact shift in the $S = \frac{1}{2}$ case, based on their dependence on the isotropic spin density around the nucleus. Phenomenologically, terms 1 and 6 are caused by the Fermi contact interaction, depending only on the spin density at the nucleus, mostly due to s orbitals. The term 3 depends on the isotropic part of $\boldsymbol{A}_{\mathrm{SO}}$, which vanishes for s orbitals. Thus, terms should be grouped based on their tensorial transform properties instead, which groups the terms 1, 3 and 6 together.

In experimental work, the paramagnetic centre is usually approximated to have a point-dipole spin distribution [5]. This corresponds to the approximation of Kurland and McGarvey [104], Eq. (3.29). Only the present term 9 has the same kind of dependence on geometry as arises from this approxima-

tion. When measured shifts are divided as per Eq. (3.30), δ^{PC} also includes the isotropic part of the novel terms 2, 4, 7, 8 and 9. Thus, suspicion is cast on whether the experimental view of pseudocontact shift is complete, and therefore whether the obtained geometric parameters are accurate. This was further explored in Paper III for a $S = 3/2$ system. In contrast, in the doublet case, only term 9 contributes to the experimental isotropic shift, in addition to the orbital and contact (1, 3 and 6) terms.

Chapter 4

Results

4.1 Background

The studied molecules were mostly selected based on their suitability for comparison with earlier computational and experimental results on ^{1}H and ^{13}C shieldings in paramagnetic systems (Paper I), and to demonstrate the new contributions arising from the theory, in Papers II and III. The exception is the boron system in Paper IV, where the main motivation was the joint experimental and computational effort to confirm the assignment of ^{11}B signals.

The nitroxide radical N6 (Fig. 4.1) had been studied experimentally by Heise *et al.* in 1999 [111] and computationally by Rinkevicius *et al.* in 2003 [18], at the nonrelativistic Ramsey/McConnell level of shielding theory which includes leading-order orbital shielding, the Fermi contact shift and spin-dipole anisotropy, but does not include the effect of using the full g-tensor instead of g_e.

The metallocenes (Fig. 4.1) were chosen for study as quintessential organometallic compounds, with the added benefit of having 10 magnetically equivalent nuclei of both carbon and hydrogen, which allows for averaging pNMR shieldings over these centres. This method has an experimental justification, as the measured shieldings are ensemble averages over internal molecular motion, and a calculation for a single nuclear position only probes

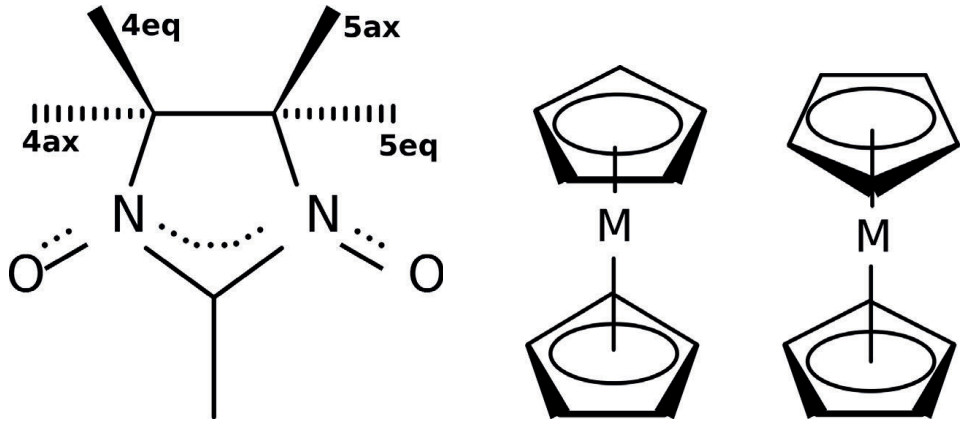

Figure 4.1: Nitroxide radical N6 studied in Paper I (left), and the eclipsed (centre) and staggered (right) conformations of a metallocene. In Paper I M=Co, Rh, Ir; in Paper II, M=Ni, Cr, Mn, V.

a single value in the ensemble. The $S > 1/2$ metallocenes in Paper II were computationally studied by Hrobárik *et al.* in 2007 employing a more limited, *a posteriori* shielding theory [25].

The chromium complexes in Papers II (Fig. 4.2) and III (Fig. 4.2) showcase the magnitude of the new contributions, introduced in Paper II, in systems without any molecular symmetry higher than C_1. In addition, the systems in Paper III demonstrate a case where the usual experimentalist definition of pseudocontact fails to include relevant physical effects present in the system.

The metallocarborane system studied in Paper IV (Fig. 4.3) has metallocene-like bonding of the open 5-ring faces of the dicarbollide moieties to the central iron atom. It was the first paramagnetic boron compound for which the NMR properties were studied jointly with modern computational methods and experiments.

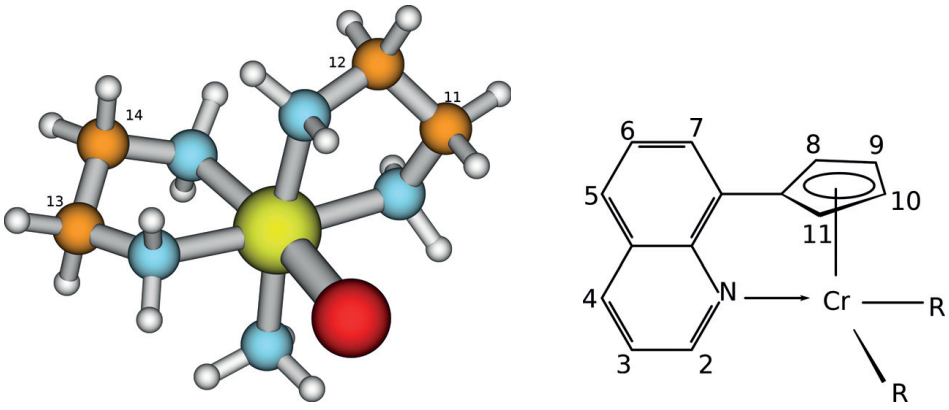

Figure 4.2: $[Cr(en)_2NH_3Br]^{2+}$, the chromium complex studied in Paper II(left) and the atom labelling scheme of the chromium complexes studied in Paper III (right). In molecule 1 of that work, R=Cl; in molecule 4, R=Br.

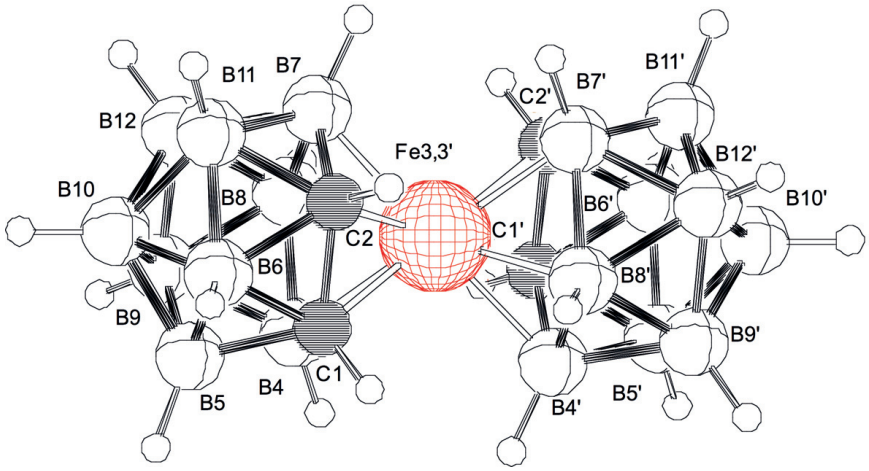

Figure 4.3: Conventional atom numbering in $[3\text{-}Fe^{III}\text{-}(1,2\text{-}C_2B_9H_{11})_2]^-$, molecule 1 of Paper IV. *Reproduced by permission of the PCCP owner societies.*

4.2 Computational methods

4.2.1 New programs

As there was no implementation available which had both the $\boldsymbol{A}_{\mathrm{SO}}$ tensors required for the new shielding terms of Paper I and a robust, well-performing SCF part, it was decided that the KS orbitals would be transformed to deMon for property calculations using an interface parser programmed by the present author. The deMon-ESR-NMR suite was, likewise, modified to calculate the new shielding contributions from SO effects (terms 3-5, 8 and 9 in Table 3.2). Another interface program was made for conveying A_{con} and $\boldsymbol{A}_{\mathrm{dip}}$ from Gaussian03 to deMon, for use with the GGAm method, see Section 4.2.2.

To be able to calculate ZFS tensors for Paper II, the property code was switched to Orca [102], which also allowed the use of hybrid functionals and higher than d angular momenta. To obtain better results for $\boldsymbol{\sigma}_{\mathrm{orb}}$, Gaussian03 was chosen for its implementation of the GIAO method. This required a new interface parser, and a separate shielding analysis program, as there is no functionality for pNMR shieldings in Orca.

For Papers II, III and IV, the results from Orca [102] and Gaussian03 were parsed and the shielding terms constructed from these components with programs made by the author. The parser is written in PERL and it is easily expandable without low-level coding to obtain the required property tensors from the output of different codes, even from separate calculations. As a demonstration of this ability, see Tables 4.8 and 4.9, where an experimental D-value was used for a ZFS tensor instead of a calculated tensor.

The new programs perform well, and the preceeding quantum-chemical calculation of property tensors is always the dominating factor for the used cpu-time.

4.2.2 Property calculations

In Paper I, the deMon-ESR-NMR program suite [17] was used for orbital shielding and most of the hyperfine calculations. As hybrid functionals could not be employed in deMon, the GGAm method was used instead. In this method, the nonrelativistic hyperfine terms, A_{con} and $\boldsymbol{A}_{\mathrm{dip}}$, were calculated in Gaussian03 with the B3LYP [112, 113] functional and used to replace the same in deMon property calculation using a GGA functional, while orbital shielding was still calculated using deMon and GGA. The sensitivity of A_{con} to the choice of functional had been explored before by Rinkevicius *et* al. [18], and the aim was to obtain better results than with GGA functionals.

As f or higher angular momenta could not be used in either deMon or its Master property code, pseudopotentials were used for the heaviest central metals. For the pseudopotential property calculations, the Stuttgart group scalar relativistic (SR) and SO pseudopotentials were used for the metals [79, 114]. The SR pseudopotentials were chosen as they include part of the relativistic effects otherwise absent at the 1-component level.

For Papers II, III and IV, $\boldsymbol{\sigma}_{\mathrm{orb}}$ was obtained from Gaussian03; $\boldsymbol{g}$, $\boldsymbol{A}$ and $\boldsymbol{D}$ were calculated with Orca [102].

In deMon, the gauge-dependent part of $\boldsymbol{\sigma}_{\mathrm{orb}}$ was calculated using the individual gauge for the localized orbitals (IGLO) method [58], as opposed to Gaussian03, which employs gauge-including atomic orbitals (GIAO) [115]. GIAO is generally perceived to perform better than IGLO, but as the paramagnetic chemical shifts are mainly due to hyperfine effects, this was not considered a central problem in this work.

The implementations of the nonrelativistic $\boldsymbol{A}$ terms are straightforward as these are first-order properties and, as such, easy to calculate as expectation values of the relevant operators over the occupied orbitals. In both deMon [116, 117] and Orca, the SO part was approximated using mean-field methods [74, 118].

The implementation of g-tensor in deMon did not have the two-electron gauge correction terms, but Orca had a mean-field implementation. The rest

of the α^2 one- and two-electron terms were present in both programs. [82, 118]

The implementation of the $\boldsymbol{D}$ tensor in ORCA is one of the few available, it includes the spin-spin part rigorously, and the SO-part with the mean-field approximation. [101, 119] The $\boldsymbol{D}$-tensor is computationally difficult, especially with DFT, and there have been systematic errors in the implementations, compare the SO-part prefactors in Ref. [120] to those found in Ref. [101], and see appendix B.

TMS has been used as the reference compound for the ^{1}H and ^{13}C nuclei throughout this work. For the ^{11}B shifts in paper IV, $BF_3{\cdot}OEt_2$ was used to set the origin of the scale in experimental work, but to obtain more reliable computational results, B_2H_6 was used as an indirect reference by setting its chemical shift to 16.6 ppm. Throughout the work, the orbital shieldings for the reference compounds were obtained with methods similar to those employed for the studied systems.

4.2.3 Partial geometry optimization

The NMR spectra of paramagnetic species are often recorded from solid-state samples. As the molecular geometry in a crystal is affected by the matrix, a geometry optimization *in vacuo* produces slightly different results. The customary experimental method of structural studies in crystalline solids is X-ray spectroscopy. As the signal strength in an X-ray measurement depends on nuclear charge, hydrogen atoms produce weak signals, and their positions are usually not reported. In Paper III, alternative geometries were obtained by starting from the X-ray structure reported by Refs. [16, 121] and optimizing only the positions of the hydrogen atoms. This method produced ^{1}H chemical shifts values generally better than those obtained with a fully relaxed geometry.

4.2.4 Thermal and solvent effects

A quantum chemical calculation is usually performed *in vacuo*, ignoring also any internal motion of the system, even the zero-point vibrations. As mag-

netic properties are sensitive to both the electronic structure and nuclear positions, these deviations from experiment should be accounted for.

In Paper IV, the thermally induced internal motion was estimated by taking snapshots from an MD simulation trajectory obtained using the leapfrog algorithm [122] as implemented in Turbomole.

The solvent effects were estimated by performing additional property calculations using the COSMO solvation model [26] with appropriate dielectric constant values for the solvents used for the associated experimental work.

4.3 Chemical shifts

As shown in Section 3.5, accurate hyperfine tensors $\boldsymbol{g}$, $\boldsymbol{A}$ and $\boldsymbol{D}$ are essential for quantitatively predicting chemical shifts in paramagnetic systems. Calculations with highly correlated wave function methods have shown that the basic physics behind $\boldsymbol{g}$ and $\boldsymbol{A}$ is well-understood, and the main problem remaining is their calculation in large systems. If DFT is used, the choice of functional is a pivotal question, both of the class (*e.g.* GGA or hybrid) of the functional, and among the hybrid functionals, the fraction of exact exchange included. For $\boldsymbol{D}$, the problems are still at a more profound level, including confusion on how it should be defined [123]. For systems with fourth-row and heavier elements, another question to be considered is whether or not the heavy atoms should be handled with pseudopotentials, when available in the implementation.

4.3.1 $S = 1/2$ systems

Arbuznikov *et al.* had shown [100] that SO effects are important for $\boldsymbol{A}$ of light elements in systems containing heavy elements. For this reason, they were included in the definition of pNMR shielding in Paper I. The effect of hybrid functionals was approximated with the GGAm method (p. 44). The error due to using a pseudopotential was estimated by performing the calculations for $RhCp_2$ both as all-electron and with Stuttgart ECPs in both

SCF (both SR and NR ECP) and property calculations (SO ECP). The new SO shielding terms were found to be significant, up to about half of $\boldsymbol{\sigma}_{\mathrm{orb}}$ for $RhCp_2$ and $IrCp_2$. GGAm performed ambivalently, improving the results for the nitroxide radical N6, but moving them outside the range of experimental literature values for $CoCp_2$. The pseudopotential calculations showed a deviation of about 5–10% from all-electron results, *vide infra* for details.

4.3.2 ZFS effects

The theory presented in Paper I was consistent for its handling of hyperfine terms up to α^4, but it was still limited to $S = 1/2$ systems. Meanwhile, Hrobárik *et al.* presented their *a posteriori* method [25] of handling the arbitrary spin state case, but in addition to not being *a priori* designed for $S > 1/2$ systems, it was limited to systems with cylindrical symmetry.

In Paper II, a more flexible and general theory for hyperfine NMR shielding was developed, allowing for arbitrary spin state and molecular symmetry, and rigorously including the effect of zero-field splitting (ZFS). It turns previously isotropic or (symmetrically) anisotropic terms into mixed tensorial rank forms. The new isotropic parts induced by ZFS (terms 2, 4, 7 and 8 in Table 3.2) would in an experiment be included in the pseudocontact shift. This conflicts with the usual experimental definition. As shown in Table 4.1, the ZFS terms were indeed found to be of comparable magnitude as the one that includes the experimentally defined pseudocontact, term 9, casting suspicion on the validity of geometry determination based on pseudocontact.

Figure 4.4 shows a comparison of the calculated ^{13}C and ^{1}H chemical shifts in metallocenes to experimental values of Refs. [19, 21, 23, 25, 124, 125, 126, 127]. The agreement is decent for the ^{13}C shifts, but it is significantly better for the ^{1}H shifts. This is possibly due to better description of Fermi contact contributions than of the other effects, of which SO effects are virtually nonexistent for hydrogen. The agreement of ^{13}C results is also best for $CoCp_2$, which is a doublet system. Therefore it is unaffected by inaccuracies in the

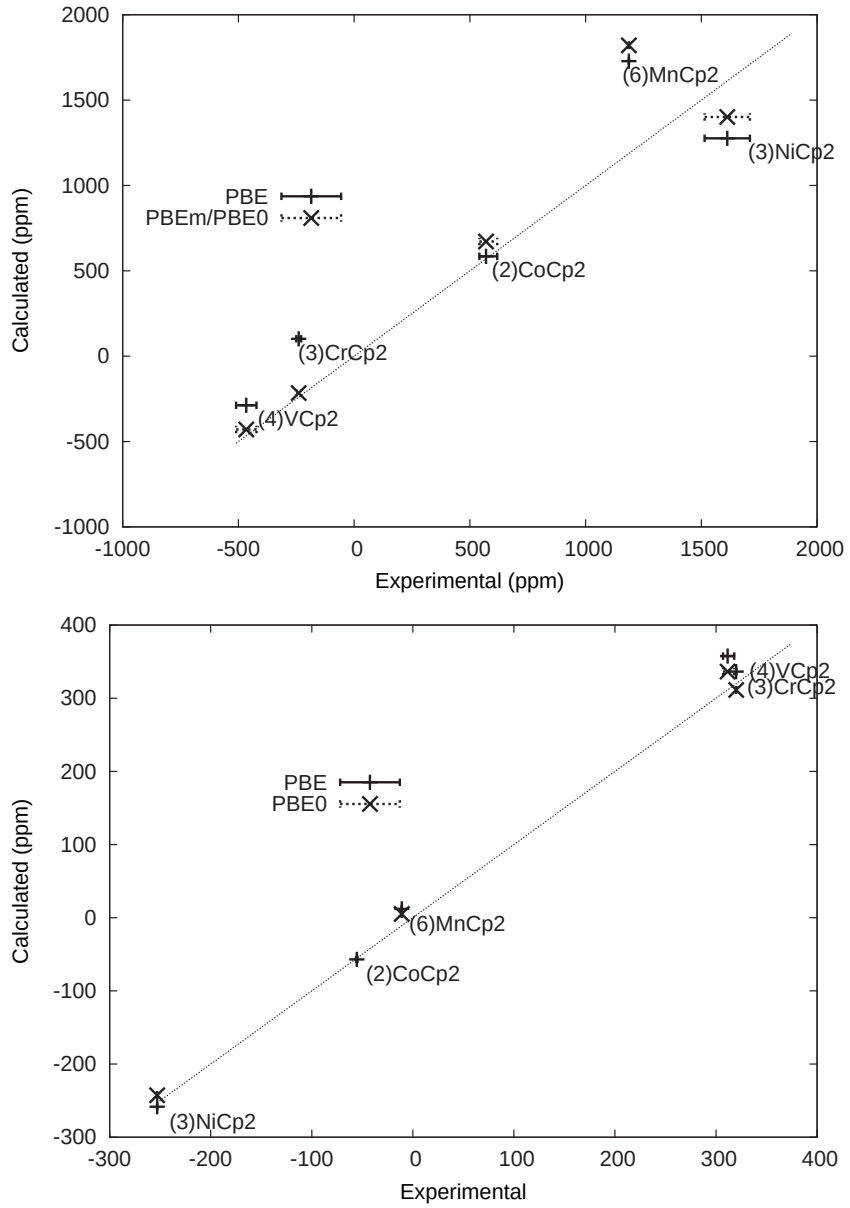

Figure 4.4: Calculated ^{13}C (above) and ^{1}H (below) chemical shifts in staggered geometry metallocenes (spin multiplicities in parenthesis), plotted against the range and average of experimental values in references. At 298K, with TMS as the reference compound. HIII basis set used for all calculations. PBE and PBE0 functionals used, except for the $CoCp_2$ PBEm result, where the isotropic A_{con} constants and the $\boldsymbol{A}_{\mathrm{dip}}$ tensors were calculated using B3LYP and the rest of the calculation was done with PBE. The diagonal line represents ideal agreement between calculated and experimental results.

calculation of zero-field splitting.

A breakdown into terms (numbered as in Table 3.2) of the calculated chemical shifts for selected representative nuclei in systems studied throughout the work can be seen in Table 4.1. For the doublet systems, terms 2, 4, 7 and 8 do not have an isotropic part as there is no ZFS present. Nitroxide radical N6 is a typical organic radical, where Fermi contact contribution (as seen in term 1) can be dominating, but SO contributions (term 3) are rather weak in comparison, as they are of relativistic origin, and there is no heavy central ion present. In contrast to the main-group system N6, Mol. 1 of Paper IV and $CoCp_2$ are transition metal systems. Consequently, the SO terms are stronger as compared to the Fermi contact contribution than in N6. $CrCp_2$ has $S = 1$, but due to weak zero-field splitting, the new terms of Paper II are nearly zero. In the chiral chromium system of Paper II, ZFS is stronger and thus the new isotropic shielding terms (2, 4, 7 and 8) are comparable to the traditional pseudocontact term 9. In Molecule 4 of Paper III, the sum of these new pseudocontact terms is larger than term 9, which is often in experimental work misinterpreted to form the whole of pseudocontact shift. It is clear that neglecting the new terms introduced in Papers I and II introduces large errors, in some cases larger than the orbital shift.

The general, rather large inaccuracy present in the DFT calculation of $\boldsymbol{D}$ compared to experimental results prompted the authors of Ref. [110] to request calculations on representative systems from Paper II using experimental D-values*, and the following results were communicated to them. These are presented as Table 4.2 to show that even with any error in the D-tensor eliminated, the new contributions still remain significant. The listed terms are those defined as pseudocontact in the present work, namely the new isotropic terms 2, 4, 7 and 8 introduced in Paper II; and term 9, which is mixed-rank already at the theory level of Paper I. The isotropic part of the contact terms 3 and 6 was not significantly affected by the changed D-value. The other terms (orbital shift and isotropic part of term 1) do not

*The experimental D-value is the anisotropy of the D-tensor, defined as $D = D_{zz} - \frac{1}{2}(D_{xx} + D_{yy})$ where D_{zz} is the diagonal component with largest absolute value.

Table 4.1: Chemical shift break-down for selected nuclei and systems. At 298 K, in ppm.[a]

			Contribution[b]									
System	Paper	Nucl.	Orb	1	2	3	4	6	7	8	9	Sum
^{2}N6[c,i]	I	C2	157.7	-2044.2	-	3.7	-	-4.4	-	-	2.3	-1884.9
$^{2}CoCp_2$(AE)[c,d,i]	I	C	105.4	516.0	-	-26.5	-	-27.1	-	-	-58.1	509.7
$^{2}CoCp_2$(NR)[c,e,i]	I	C	105.1	515.7	-	-4.0	-	-24.5	-	-	-52.4	539.9
$^{2}CoCp_2$(SR)[c,f,i]	I	C	103.2	527.6	-	-3.9	-	-25.8	-	-	-50.5	550.6
$^{3}CrCp_2$[g,i]	II	C	107.7	-226.0	0.0	18.8	0.0	-1.9	0.0	0.0	-0.7	-102.0
$^{6}[Cr(en)_2BrNH_3]^{2+}$[g,i]	II	C_{11}	36.44	1549.67	-162.68	-549.66	-202.6	399.12	-41.90	106.02	-62.10	1282.31
^{4}Mol. 4[h,j]	III	H_2	8.5	-124.7	-16.1	2.1	-0.0	-0.5	-0.1	0.0	1.7	-128.9
^{2}Mol. 1[g,j]	IV	$B_{8/8'}$	17	-430.2	-	10.8	-	-23.5	-	-	2.4	-457±7[k]

[a]Orbital shielding reference compound is TMS for ^{13}C and ^{1}H shifts and B_2H_6 @16.6 ppm for ^{11}B shifts. [b]Terms numbered as in Table 3.2. [c]BP86 functional [128, 129]. [d]All-electron calculation. [e]Non-relativistic Stuttgart pseudopotential. [f]Scalar relativistic Stuttgart pseudopotential. [g]PBE functional [130]. [h]B3LYP functional [112, 113]. [i]HIII basis set [65, 58]. [j]HII basis set [65, 58]. [k]Includes basis set correction to HIII+d1 (one additional diffuse valence function) calculated with the PBE functional, error bars and corrections obtained from MD and solvation effects estimated by the COSMO model [26].

Table 4.2: ^{13}C and ^{1}H total chemical shifts and shielding terms 2, 4, 7, 8 and 9 in ppm at 298 K calculated using the PBE0 functional and HII basis set for the electronic structure and either calculated or experimental D-values.

			σ term					
		D (cm^{-1})	2	4	7	8	9	δ
^{3}NiCp$_2$ Paper II	^{13}C	104	196.2	3.4	4.2	-3.0	21.3	1401.2
Exp. D-value	^{13}C	30	54.0	0.9	1.2	-0.8	22.8	1545.2
^{3}CrCp$_2$ Paper II	^{13}C	-2	0.3	-0.0	0.0	0.0	2.2	-215.9
Exp. D-value	^{13}C	-15	1.9	-0.1	0.1	2.2	2.2	-217.6
^{3}NiCp$_2$ Paper II	^{1}H	104	0.2	0.2	0.0	0.5	0.0	-242.6
Exp. D-value	^{1}H	30	0.1	0.1	0.0	0.1	0.0	-242.0
^{3}CrCp$_2$ Paper II	^{1}H	-2	-0.1	0.0	0.0	-0.0	-0.6	311.3
Exp. D-value	^{1}H	-15	-0.5	0.0	-0.0	-0.1	-0.6	311.8

vary with D at all. The difference in terms 2, 4, 7 and 8 is for the most part approximately linear with the difference in D.

4.3.3 Choice of functional and basis

From the previous experience in Papers I and II, the hyperfine tensors were known to depend heavily on whether or not the exchange-correlation functional used had exact exchange or not. This raised the question of how the amount of exact exchange would affect the results. Also, basis set effects were well-known for the orbital shift in diamagnetic compounds, but no comprehensive study existed for paramagnetic systems. Additional tests of the theory presented in Paper II were performed in Paper III on a set of high-spin compounds without axial symmetry.

Table 4.3 shows the effect of functional choice on g- and D-tensor principal values for Mol. 4 of Paper III. The general trend is towards decreasing g-shifts and stronger zero-field splitting with increasing amount of exact exchange in the functional.

The effect of the functional choice on the total chemical shifts in Paper IV can be seen in Table 4.4. As seen before from Table 4.3, the ESR tensors depend significantly on the amount of exact exchange in the functional.

Table 4.3: g and $\boldsymbol{D}$ tensor principal values for Mol. 4 of Paper III. Calculated using the HII basis set. $\boldsymbol{D}$ tensor values in cm^{-1}.

Property	Funct.	Principal values		
$\boldsymbol{g}$	PBE[a]	2.0087	2.0105	2.0256
	PBE0[a]	1.9994	2.0040	2.0175
	BLYP[b]	2.0100	2.0118	2.0275
	B3LYP[c]	2.0021	2.0063	2.0206
	BHandHLYP[d]	1.9928	1.9990	2.0129
$\boldsymbol{D}$	PBE	-210.76	-207.08	-203.66
	PBE0	-288.58	-272.59	-257.08
	BLYP	-210.23	-206.53	-202.83
	B3LYP	-263.74	-257.84	-244.94
	BHandHLYP	-371.42	-231.48	-218.37

[a]Ref. [130]. [b]Refs. [128, 131]. [c]Refs. [112]. [d]Refs. [131, 132].

Table 4.4: Effect of functional on chemical shift. At 298 K, in ppm. Shielding reference compound is TMS for ^{13}C shifts, B_2H_6 @16.6 ppm for ^{11}B shifts.

			Functional					
System	Paper	Nucleus	BP86[a]	BP86m[b]	PBE[c]	PBE0[d]	B3LYP[e]	BHandHLYP[f]
^{2}N6[g]	I	C2	-1884.9	-3714.5	-2036.4	-	-	-
^{2}CoCp$_2$[g]	I	C	550.8	678.9	586.1	-	-	-
^{3}CrCp$_2$[g]	II	C	-	-	-102.0	-215.88	-	-
^{2}Mol. 1[h]	IV	$B_{8/8'}$	-	-	-457±7	-689±7	-620±7	-1030±7

[a]Refs. [128, 129]. [b]A_{con} and $\boldsymbol{A}_{\mathrm{dip}}$ calculated using B3LYP functional, everything else with BP86 functional. [c]Ref. [130]. [d]Ref. [130]. [e]Ref. [112]. [f]Becke's half-and-half exchange functional [132] combined with Lee-Yang-Parr correlation part [131]. [g]HIII basis set. [h]HII basis set with basis set correction to HIII+d1 (one additional diffuse valence function) calculated with PBE functional, error bars and corrections obtained from MD and solvation effects estimated by the COSMO model.

As a direct consequence, similar dependence can be seen in total chemical shifts constructed with them. This shows clearly the uncertainty in hyperfine properties due to choice of functional, despite the generally good DFT results obtained in other properties such as molecular geometries and energetics. This is possibly due to the generation process of functionals: For example, error cancellation finely tuned by the optimization of the semi-empirical parameters against total energy or geometry results (both dictated by valence behaviour) does not work so well for the properties arising from the core region (especially the Fermi contact interaction).

The basis set dependence of chemical shifts in Mol. 1 of Paper III can be seen in Table 4.5. The HIII basis set already produces results as good as the largest basis sets tested, but this is likely due to error cancellation. Compared to the error due to functional choice, as seen in Table 4.4 and by comparing to experimental results in Table 4.5, it can be seen that the basis set errors are insignificant already at the HIIIt3 level. This occurs although the results obtained with Huzinaga-Kutzelnigg basis sets for the separate hyperfine properties are not near basis set limit, and it is due to error cancellation. The inaccuracy originating in the functionals further distorts the results, causing the agreement with experimental results to be only qualitative.

Table 4.5: Effect of basis set used for main group elements on the ^{1}H chemical shift in Molecule 1 of Paper IV, $S = \frac{3}{2}$. At 298 K, in ppm, TMS as the shielding reference compound. With the B3LYP functional.

Nucleus	Exp.[a]	HII[b]	HIII[b]	HIIIt1[c]	HIIIt2	HIIIt3	HIIIt4	HIV[b]	HIVt1	HIVt2
2	-78.0	-181.9	-167.7	-174.3	-177.9	-180.0	-181.1	-176.8	-178.0	-184.7
3	51.8	79.0	74.3	76.6	78.0	78.8	79.2	79.1	79.7	82.4
4	-56.0	-152.3	-134.9	-141.9	-143.9	-146.3	-146.7	-147.9	-148.8	-154.8
5	-15.8	-42.1	-37.1	-38.8	-39.8	-40.3	-40.6	-38.9	-39.7	-41.5
6	15.3	16.8	14.0	14.4	14.4	14.5	14.5	15.2	15.4	15.7
8/11	27.6	56.3	55.2	56.5	58.1	58.4	58.9	60.1	60.8	62.8
9/10	-41.1	-31.1	-29.3	-29.7	-30.7	-30.9	-31.2	-27.2	-27.8	-28.8

[a]Ref. [16]. [b]Refs. [65, 58]. [c]tN basis sets have N sets of additional tight s and p type functions for the hydrogens.

4.3.4 Vibrational and solvation corrections

In Paper IV, the emphasis was moved almost completely from the testing of the theory itself to the effects of method choice (functional and basis) and deviations from the static *in vacuo* picture. In addition, there was associated experimental work, the results of which were interpreted in the light of the computational work. The corrections were estimated by calculating the difference that these introduce to the results at a computationally cheap theory level (HII/PBE), then these were considered as additivie corrections to

Table 4.6: Combined effect of different corrections on the ^{11}B chemical shift in Molecule 1 of Paper IV with HII basis set, $S = \frac{1}{2}$. Atoms numbered as in Fig. 4.3. At 298 K, in ppm.[a]

	Functional/Correction						
Boron atom	PBE	PBE0	Basis[b]	MD[c]	COSMO[d]	PBE+[e]	PBE0+[e]
8,8'	-426.3	-657.9	12.6	-24	-20	-457±7	-689±7
4,7,4',7'	-508.4	-718.8	12.5	36	-6	-464±5	-674±5
5,11,5',11'	-15.6	-31.0	0.6	-26	-3	-20±3	-35±3
9,12,9',12'	-20.4	-3.4	-0.5	8	-3	16±2	1±2
10,10'	-71.5	-79.2	1.6	-31	-1	-102±1	-110±1
6,6'	5.9	46.3	-3.8	68	3	72±4	113±4

[a]Shielding reference compound is B_2H_6 @16.6 ppm. [b]Difference between HIII+d1 (one additional diffuse valence function) and HII results, calculated with the PBE functional. [c]Average of 20 MD snapshots compared to optimized geometry. [d]Solvation corrections obtained by comparing HII results to ones calculated with the COSMO solvation model. [e]Sum of appropriate base results and corrections, with MD error bars.

the base calculations with HII and PBE/PBE0. The MD vibrational corrections obtained here are smaller than would be expected from a QM analysis of vibrational modes and related corrections to the probability distribution of geometries in the ensemble, as zero-point vibration is not present in the model. Likewise, the results obtained with a solvation model are only trend-setting compared to an explicit solvent with dynamics. The corrections due to different computational method choices are shown in Table 4.6 for Mol. 1 of Paper IV. Generally, the vibrational corrections (as estimated by MD methods) are larger than basis set errors or solvent effects (as estimated by the COSMO model). However, while significant, all these are dwarfed, again, by errors due to choice of functional. The basis set errors are largest for sites near the metal centre.

4.3.5 Nuclear shielding anisotropies

Shielding anisotropy is measured from suspended (*e.g.*, solid or liquid crystal) samples as it provides additional information about the environment of the nucleus. The anisotropies throughout this work are defined as $\Delta\sigma =$

$\sigma_{zz} - \frac{1}{2}(\sigma_{xx} + \sigma_{yy})$, where the σ_{aa} are the principal aa components of the diagonalized shielding tensor. Table 4.7 shows a comparison of ^{13}C shielding anisotropies in metallocenes obtained with PBE and PBE0 functionals and experimentally. The agreement with experiment is at least qualitative, but once again, there is a large difference between the results of the GGA and the hybrid functionals.

Break-downs of ^{13}C and ^{1}H shielding anisotropies in the group 9 metallocenes of Paper I are shown in Tables 4.8 and 4.9, respectively. The pseudopotential calculations are not entirely comparable with the all-electron ones due to approximated core region in ECP and lack of scalar relativistic effects in all-electron calculations, but trends can be seen by comparing them as separate pairs. The carbon shielding anisotropy is dominated by the leading order spin-dipole contribution (term 2 in Table 3.2, with sizeable contributions from orbital shielding and g-shift (terms 7–9). The isotropic part of g-shift (term 7) becomes more important with a heavier metal centre. This is due to its dependence on the SO part of g-tensor. For hydrogen shielding, g-shift (especially term 8) is the dominant term at the light end of the group, while the dipolar term 2 reaches equal strength at the heavy end.

Table 4.7: ^{13}C shielding anisotropies from all-electron calculations on metallocenes with the HIII basis set; and the corresponding experimental values from literature. At 298 K, in ppm.

	Functional		
System	PBE	PBE0	Exp.[a]
$^{2}CoCp_2$(ecl)	-658.9		-443
$^{2}CoCp_2$(stag)	-653.2		-443
$^{3}NiCp_2$	-3901.47	-2509.73	-2855
$^{3}CrCp_2$	148.35	299.65	
$^{4}VCp_2$	-899.42	-645.05	-831
$^{6}MnCp_2$	-5074.43	-4238.57	

[a] Ref. [19].

Table 4.8: Corrected[a] Table VI from Paper I, ^{13}C shielding anisotropies of metallocenes calculated with the PBE functional and HIII basis set, in ppm at 298K.

	Chemical shift term[b]						
	orb	dip(2)	dip,2(4)	dip,3(7)	c,aniso(8)	pc(9)	Sum
$CoCp_2$(ecl)	83.24	-839.01	2.69	14.31	52.01	27.82	-658.94
$CoCp_2$(stag)	84.07	-834.96	2.56	14.3	52.71	28.12	-653.2
$RhCp_2$(ecl)AE[c]	91.7	-1353.35	-1.2	71.22	109.72	86.57	-995.35
$RhCp_2$(stag)AE	92.2	-1351.53	-1.54	70.7	109.69	86.94	-993.55
$RhCp_2$(ecl)PP[d]	89.2	-1295.34	-1.59	64.5	102.56	76.12	-964.55
$RhCp_2$(stag)PP	89.82	-1293.56	-1.67	64.32	102.67	76.51	-961.92
$IrCp_2$(ecl)PP	85.29	-1266.3	-2.28	86.09	81.26	46.52	-969.43
$IrCp_2$(stag)PP	86.87	-1242.05	-2.2	102.74	109.56	59.51	-885.58

[a]Anisotropies from shielding tensors averaged for the ten equivalent nuclei after transforming the tensors to same orientation. [b]Labelled as in table 3.2. [c]All-electron calculation. [d]Calculation using the Stuttgart group scalar relativistic pseudopotentials.

Table 4.9: Corrected[a] Table VII from Paper I, ^{1}H shielding anisotropies of metallocenes calculated with the PBE functional and HIII basis set, in ppm at 298K.

	Chemical shift term[b]						
	orb	dip(2)	dip,2(4)	dip,3(7)	c,aniso(8)	pc(9)	Sum
$CoCp_2$(ecl)	-1.57	-1.74	-2.3	0.05	-6.27	-0.08	-11.91
$CoCp_2$(stag)	-1.6	-2.19	-2.32	0.05	-6.34	-0.07	-12.47
$RhCp_2$(ecl)AE[c]	-1.12	-4.08	-4.29	0.18	-18.67	-0.01	-27.99
$RhCp_2$(stag)AE	-1.2	-4.16	-4.35	0.22	-18.74	-0.02	-28.25
$RhCp_2$(ecl)PP[d]	-1.37	-5.01	-0.45	0.25	-16.54	0.07	-23.05
$RhCp_2$(stag)PP	-1.46	-5.08	-0.45	0.26	-16.63	0.05	-23.31
$IrCp_2$(ecl)PP	-1.64	-10.44	-0.24	0.73	-10.7	-0.72	-23.01
$IrCp_2$(stag)PP	-1.62	-9.64	-0.26	0.79	-13.44	-0.27	-24.44

[a]Anisotropies from shielding tensors averaged for the ten equivalent nuclei after transforming the tensors to same orientation. [b]Labelled as in table 3.2. [c]All-electron calculation. [d]Calculation using the Stuttgart group scalar relativistic pseudopotentials.

Chapter 5

Conclusions

The aim of this work was to present a rigorous theory for NMR shielding in paramagnetic compounds, consistently including hyperfine shielding terms arising from the BP Hamiltonian up to total order $\mathcal{O}(\alpha^4)$. A further goal was to allow arbitrary spin state to replace the former theory which only allowed for a doublet case. In paper I, hyperfine SO effects were added to the earlier formulation of Moon and Patchkovskii, which was for the first time consistently implemented in a quantum-chemical code. The theory was reformalized to allow arbitrary spin state in Paper II, where the leading-order magnetic field dependence of hyperfine shielding was also derived (but not implemented). As a consequence of including ZFS effects, the previously purely isotropic or (symmetric) anisotropic shielding terms were generalized to have mixed tensorial rank, as shown in Table 3.2. The new theory was tested by performing DFT property calculations on a representative set of compounds. The group of new contributions to paramagnetic chemical shift has been shown to be significant, of equal magnitude with the orbital shielding. In some cases, especially further away from the paramagnetic centre, these can even be equal to the usually dominant Fermi contact shift. Of special interest is the observation that while the experimentalist view of pseudocontact shift, based on the point-like dipole approximation of the spin distribution, only consists of what is included in term 9 (actual pseudocontact) in this work, in actual measurements consists of the isotropic part of terms 2 (non-

relativistic dipolar term), 4 (SO correction to 2), 7 (isotropic g-shift/dipolar hyperfine term), 8 (anisotropic g-shift/hyperfine contact term) and 9. As the measured pseudocontact shift is used for the analysis of geometry, this flaw in the definition can lead to erroneous results.

In general, the ESR property tensors, and as a result the chemical shift, show a strong dependence on the amount of exact exchange in the exchange-correlation functional used. The greatest dependence for DFT calculations of hyperfine NMR shifts being calculating A_{con} and $\boldsymbol{D}$. None of the functionals tested have given reliable results for all of the required properties for transition metal systems. This underlines the importance of seeking better DFT functionals.

A moderate amount (25-30%) of exact exchange generally gives better results (even if there is no specific amount that can be said to be optimal). On the other hand, using a hybrid functional makes the scaling of computational effort much worse because iterative coupled-perturbed calculations are required for each degree of freedom in the perturbation, 3 for g, $\boldsymbol{D}$ or $\boldsymbol{\sigma}$, and $3N$ for $\boldsymbol{A}_{\mathrm{SO}}$ (N is the number of nuclei for which the calculation is made). As a result, the rather small basis set error from the HII or HIII basis set may be a more than acceptable tradeoff.

At the most basic level, the theory of paramagnetic shielding presented in this work only depends on the accuracy of the EPR tensors, and as such, future efforts should be concentrated on improving the methods for obtaining them. Another direction for the next step ahead would be the additional properties required for proper calculation of the leading-order magnetic field dependence of shielding.

Appendix A

Tensors

Some physical properties, such as the rest mass of an object, are independent of the coordinate system in which we are observing them. These properties are isotropic, and can be described by a single number, a scalar. Some, such as momentum, also have a direction, so they have to be described by a vector. Other properties, such as polarizability, couple a vector-represented cause to a vector-represented effect (not necessarily in the same direction). * Thus, they require a matrix for an adequate description. All these three are examples of a more general concept of tensor, namely rank-0, rank-1 and rank-2 tensors. The magnetic properties $\boldsymbol{\sigma}$, $\boldsymbol{g}$, hyperfine coupling $\boldsymbol{A}$ and zero-field splitting $\boldsymbol{D}$ handled in this work are treated as (matrix-formed) tensors which can be divided into sums of terms up to second rank. The isotropic rank-0 term of tensor $\boldsymbol{T}$ is defined as

$$T_{\text{iso}} = \frac{1}{3}\text{Tr}\boldsymbol{T} = \frac{1}{3}(T_{xx} + T_{yy} + T_{zz}). \tag{A.1}$$

*Polarizability represents the dependence of the direction (and strength) of polarization on the direction of the polarizing electric field, $\boldsymbol{p} = \boldsymbol{\alpha}\boldsymbol{\mathcal{E}}$, where $\boldsymbol{p}$ is the polarization vector, $\boldsymbol{\mathcal{E}}$ is the electric field vector and $\boldsymbol{\alpha}$ is the polarizability tensor.

The anisotropic remainder can be further divided into symmetric (s, rank-2) and antisymmetric (as, rank-1) parts,

$$\begin{aligned} \boldsymbol{T} &= T_{\text{iso}}\mathbf{1} + \boldsymbol{T}^{\text{s}} + \boldsymbol{T}^{\text{as}}, \\ \boldsymbol{T}^{\text{s}} &= \frac{1}{2}(\boldsymbol{T} + \boldsymbol{T}^{T}) - T_{\text{iso}}\mathbf{1}, \\ \boldsymbol{T}^{\text{as}} &= \frac{1}{2}(\boldsymbol{T} - \boldsymbol{T}^{T}). \end{aligned} \tag{A.2}$$

Appendix B

Errata

Paper I

Equation (6) is missing a factor of 3 from the denominator, this is a typographical error and the numerical results include it. The correct form of the equation is:

$$\boldsymbol{\sigma}_K = \boldsymbol{\sigma}_K^{\mathrm{orb}} - \frac{1}{\gamma_K}\frac{\mu_{\mathrm{B}}}{3kT}S(S+1)\boldsymbol{g}\cdot\boldsymbol{A}_K. \tag{B.1}$$

For the less symmetric metallocenes (especially $IrCp_2$, to some extent the staggered conformation of $RhCp_2$), the anisotropies and principal components σ_{nn} of shielding listed in Tables VI and VII are incorrectly the results of diagonalization of the averaged shielding tensors for the experimentally equivalent nuclei. The correct method is to either transform the tensors into the same orientation before averaging, or to diagonalize each tensor separately and then to average the equivalent principal components. The corrected tables are included as Tables 4.8 and 4.9. The method of transforming to the same orientation and averaging before diagonalization was employed.

Papers II and III

The versions of ORCA [102] code used were reported in February 2011 to have an error in the spin-spin part of $\boldsymbol{D}$. This error affected calculations at DFT level for systems with spin density on orbitals with d or higher orbital angular momentum, *e.g.*, complexes of d-block transition metals such as studied in these papers. This mainly affects the results for shielding terms 2, 4, 7 and 8 in Table 3.2 which include isotropic parts only due to zero-field splitting effects, as well as term 9 which always has mixed tensorial rank. In transition metal compounds, as studied in this work, spin-orbit effects are overwhelmingly dominant in zero-field splitting, and thus, this error should not drastically change the results.

The author of the ORCA code notified users about this error while this summary was reaching its final version and complete corrected data are regrettably not available to be presented here.

Bibliography

[1] F. Bloch. *Phys. Rev.* **70**, 460 (1946).

[2] F. Bloch, W. W. Hansen, and M. Packard. *Phys. Rev.* **70**, 474 (1946).

[3] E. M. Purcell, H. G. Torrey, and R. V. Pound. *Phys. Rev.* **69**, 37 (1946).

[4] H. Friebolin. *Basic One- and Two-Dimensional NMR Spectroscopy.* 3rd ed. (Wiley-VCH, Weinheim, 1998).

[5] I. Bertini, C. Luchinat, and G. Parigi. *Solution NMR of Paramagnetic Molecules - Applications to Metallobiomolecules and Models*, vol. 2 of *Current Methods in Inorganic Chemistry* (Elsevier, Amsterdam, 2001).

[6] T. Hase. *Tables for Organic Spectrometry* (Otatieto, Helsinki, 2008).

[7] M. Kaupp, M. Bühl, and V. G. Malkin, (Eds.) *Calculation of NMR and EPR Parameters: Theory and Applications* (Wiley-VCH, Weinheim, 2004).

[8] J. Vaara. *Phys. Chem. Chem. Phys.* **9**, 2954 (2007).

[9] T. Helgaker, M. Jaszuński, and K. Ruud. *Chem. Rev.* **99**, 293 (1999).

[10] S. Moon and S. Patchkovskii. In *Calculation of NMR and EPR Parameters: Theory and Applications*, edited by M. Kaupp, M. Bühl, and V. G. Malkin, 325 (Wiley-VCH, Weinheim, 2004).

[11] H. M. McConnell and D. B. Chesnut. *J. Chem. Phys.* **28**, 107 (1958).

[12] H. M. McConnell and R. E. Robertson. *J. Chem. Phys.* **29**, 1361 (1958).

[13] B. Kok, B. Forbush, and M. McGloin. *Photochem. Photobiol.* **11**, 457 (1970).

[14] S. Schinzel, J. Schraut, A. Arbuznikov, P. Siegbahn, and M. Kaupp. *Chem. Eur. J.* **16**, 10424 (2010).

[15] I. Bertini, P. Turano, and A. J. Vila. *Chem. Rev.* **93**, 2833 (1993).

[16] P. Fernández, H. Pritzkow, J. J. Carbó, P. Hofmann, and M. Enders. *Organometallics* **26**, 4402 (2007).

[17] V. G. Malkin, O. L. Malkina, L. A. Eriksson, and D. R. Salahub. In *Modern Density Functional Theory: A Tool for Chemistry; Theoretical and Computational Chemistry*, edited by J. M. Seminario and P. Politzer, vol. 2 (Elsevier, 1995).

[18] Z. Rinkevicius, J. Vaara, L. Telyatnyk, and O. Vahtras. *J. Chem. Phys.* **118**, 2550 (2003).

[19] H. Heise, F. H. Köhler, and X. Xie. *J. Magn. Reson.* **150**, 198 (2001).

[20] F. H. Köhler. *J. Organomet. Chem.* **110**, 235 (1976).

[21] F. H. Köhler and W. Prössdorf. *J. Am. Chem. Soc.* **100**, 5970 (1978).

[22] H. Eicher and F. H. Köhler. *Chem. Phys.* **128**, 297 (1988).

[23] N. Hebendanz, F. H. Köhler, F. Scherbaum, and B. Schlesinger. *Magn. Reson. Chem.* **27**, 798 (1989).

[24] J. Hulliger, L. Zoller, and J. H. Ammeter. *J. Magn. Reson.* **48**, 512 (1982).

[25] P. Hrobárik, R. Reviakine, A. V. Arbuznikov, O. L. Malkina, V. G. Malkin, F. H. Köhler, and M. Kaupp. *J. Chem. Phys.* **126**, 024107 (2007).

[26] A. Klamt and G. Schüürmann. *J. Chem. Soc., Perkin Trans. 2* 799 (1993).

[27] M. Planck. *Annalen der Physik* **4**, 553 (1901).

[28] A. Einstein. *Annalen der Physik* **17**, 132 (1905).

[29] E. Schrödinger. *Annalen der Physik* **79**, 361 (1926).

[30] E. Schrödinger. *Annalen der Physik* **79**, 489 (1926).

[31] E. Schrödinger. *Annalen der Physik* **80**, 437 (1926).

[32] E. Schrödinger. *Annalen der Physik* **81**, 109 (1926).

[33] W. Heisenberg. *Z. Phys.* **33**, 879 (1925).

[34] M. Born and P. Jordan. *Z. Phys.* **34**, 858 (1925).

[35] M. Born, W. Heisenberg, and P. Jordan. *Z. Phys.* **35**, 557 (1926).

[36] P. A. M. Dirac. *Proc. Roy. Soc. A* **123**, 714 (1929).

[37] R. L. Mössbauer. *Z. Phys.* **151**, 124 (1958).

[38] National Institute of Standards and Technology. *CODATA, http://physics.nist.gov/cuu/Constants/index.html*.

[39] *CRC Handbook of Chemistry and Physics*. 91st ed. (CRC Press, Boca Raton, FL, 2010).

[40] J. E. Harriman. *Theoretical Foundations of Electron Spin Resonance* (Academic Press, New York, 1978).

[41] M. Born and R. Oppenheimer. *Annalen der Physik* **84**, 457 (1927).

[42] P. W. Atkins and R. S. Friedman. *Molecular Quantum Mechanics*. 3rd ed. (Oxford University Press, Oxford, 1997).

[43] P.-O. Widmark, (Ed.) *European Summerschool in Quantum Chemistry 2007 Book I.* 5th ed. (Lund University, Lund, 2007).

[44] C. C. J. Roothaan. *Rev. Mod. Phys.* **23**, 69 (1951).

[45] G. G. Hall. *Proc. Roy. Soc. A* **208**, 328 (1951).

[46] C. Møller and M. S. Plesset. *Phys. Rev.* **46**, 618 (1934).

[47] T. Helgaker, P. Jørgensen, and J. Olsen. *Modern Electronic-Structure Theory* (John Wiley & Sons Ltd, Chichester, 2000).

[48] J. Almlöf, K. Fægri, Jr., and K. Korsell. *J. Comput. Chem.* **3**, 385 (1982).

[49] P. Hohenberg and W. Kohn. *Phys. Rev.* **136**, B864 (1964).

[50] W. Kohn and L. J. Sham. *Phys. Rev.* **140**, A1133 (1965).

[51] J. C. Slater. *Phys. Rev. B* **81**, 385 (1951).

[52] P. A. M. Dirac. *Proc. Cambridge Phil. Soc.* **26**, 376 (1930).

[53] S. H. Vosko, L. Wilk, and M. Nusair. *Can. J. Phys.* **58**, 1200 (1980).

[54] W. Koch and M. C. Holthausen. *A Chemist's guide to Density Functional Theory* (Wiley-VCH, Weinheim, 2000).

[55] S. F. Boys. *Proc. Roy. Soc. A* **200**, 542 (1950).

[56] M. Güell, J. M. Luis, M. Solà, and M. Swart. *J. Phys. Chem. A* **112**, 6384 (2008).

[57] T. H. Dunning, Jr. *J. Chem. Phys.* **90**, 1007 (1989).

[58] W. Kutzelnigg, U. Fleischer, and M. Schindler. In *NMR Basic Principles and Progress*, edited by P. Diehl, E. Fluck, H. Günther, and R. Kosfeld, vol. 23, 165 (Springer-Verlag, 1990).

[59] M. Munzarová and M. Kaupp. *J. Phys. Chem. A* **103**, 9966 (1999).

[60] F. Jensen. *J. Chem. Theor. Comp.* **2**, 1360 (2006).

[61] F. Jensen. *J. Chem. Theor. Comp.* **4**, 719 (2008).

[62] D. P. Chong. *Can. J. Chem.* **73**, 79 (1995).

[63] P. Manninen and J. Vaara. *J. Comput. Chem.* **27**, 434 (2006).

[64] S. Ikäläinen, P. Lantto, P. Manninen, and J. Vaara. *J. Chem. Phys.* **129**, 124102 (2008).

[65] S. Huzinaga. *Approximate Atomic Functions* (University of Alberta, 1971).

[66] T. Helgaker, M. Jaszuński, K. Ruud, and A. Górska. *Theor. Chem. Acc.* **99**, 265 (1998).

[67] K. Fægri, Jr. and J. Almlöf. *J. Comput. Chem.* **7**, 396 (1986). See also http://folk.uio.no/knutf/bases/one/.

[68] E. J. Baerends, D. E. Ellis, and P. Ros. *Chem. Phys.* **2**, 41 (1973).

[69] K. Eichkorn, O. Treutler, H. Öhm, M. Häser, and R. Ahlrichs. *Chem. Phys. Lett.* **240**, 283 (1995).

[70] K. Eichkorn, F. Weigend, O. Treutler, and R. Ahlrichs. *Theor. Chem. Acc.* **97**, 119 (1997).

[71] P. Sałek, S. Høst, L. Thøgersen, P. Jørgensen, P. Manninen, J. Olsen, B. Jansik, S. Reine, F. Pawlowski, E. Tellgren, T. Helgaker, and S. Coriani. *J. Chem. Phys.* **126**, 114110 (2007).

[72] F. Weigend. *Phys. Chem. Chem. Phys.* **4**, 4285 (2002).

[73] S. Kossmann and F. Neese. *Chem. Phys. Lett.* **481**, 240 (2009).

[74] F. Neese. *J. Comput. Chem.* **24**, 1740 (2003).

[75] M. J. Frisch, G. W. Trucks, H. B. Schlegel, G. E. Scuseria, M. A. Robb, J. R. Cheeseman, J. A. Montgomery, Jr., T. Vreven, K. N. Kudin, J. C. Burant, J. M. Millam, S. S. Iyengar, J. Tomasi, V. Barone, B. Mennucci, M. Cossi, G. Scalmani, N. Rega, G. A. Petersson, H. Nakatsuji, M. Hada, M. Ehara, K. Toyota, R. Fukuda, J. Hasegawa, M. Ishida, T. Nakajima, Y. Honda, O. Kitao, H. Nakai, M. Klene, X. Li, J. E. Knox, H. P. Hratchian, J. B. Cross, V. Bakken, C. Adamo, J. Jaramillo, R. Gomperts, R. E. Stratmann, O. Yazyev, A. J. Austin, R. Cammi, C. Pomelli, J. W. Ochterski, P. Y. Ayala, K. Morokuma, G. A. Voth, P. Salvador, J. J. Dannenberg, V. G. Zakrzewski, S. Dapprich, A. D. Daniels, M. C. Strain, O. Farkas, D. K. Malick, A. D. Rabuck, K. Raghavachari, J. B. Foresman, J. V. Ortiz, Q. Cui, A. G. Baboul, S. Clifford, J. Cioslowski, B. B. Stefanov, G. Liu, A. Liashenko, P. Piskorz, I. Komaromi, R. L. Martin, D. J. Fox, T. Keith, M. A. Al-Laham, C. Y. Peng, A. Nanayakkara, M. Challacombe, P. M. W. Gill, B. Johnson, W. Chen, M. W. Wong, C. Gonzalez, and J. A. Pople. *Gaussian 03, Revision C.02*. (Gaussian, Inc., Wallingford, CT, 2004).

[76] W. D. Cornell, P. Cieplak, C. I. Bayly, I. R. Gould, K. M. Merz, Jr., D. M. Ferguson, D. C. Spellmeyer, T. Fox, J. W. Caldwell, and P. A. Kollman. *J. Am. Chem. Soc.* **117**, 5179 (1995).

[77] R. Car and M. Parrinello. *Phys. Rev. Lett.* **55**, 2471 (1985).

[78] P. Pyykkö and H. Stoll. *Relativistic Pseudopotential Calculations, 1993 - June 1999*, vol. 1 (Royal Society of Chemistry, Cambridge, 2000).

[79] D. Andrae, U. Häussermann, M. Dolg, H. Stoll, and H. Preuss. *Theor. Chim. Acta* **77**, 123 (1990).

[80] A. Bergner, M. Dolg, W. Küchle, H. Stoll, and H. Preuss. *Mol. Phys.* **80**, 1431 (1993).

[81] F. Neese. *Coord. Chem. Rev.* **253**, 526 (2009).

[82] F. Neese. *J. Chem. Phys.* **115**, 11080 (2001).

[83] G. Breit. *Phys. Rev.* **34**, 553 (1929).

[84] L. L. Foldy and S. A. Wouthuysen. *Phys. Rev.* **78**, 29 (1950).

[85] N. F. Ramsey. *Phys. Rev.* **89**, 527 (1953).

[86] J. Vaara, P. Manninen, and P. Lantto. In *Calculation of NMR and EPR Parameters: Theory and Applications*, edited by M. Kaupp, M. Bühl, and V. G. Malkin, 209 (Wiley-VCH, Weinheim, 2004).

[87] M. Blume and R. E. Watson. *Proc. Roy. Soc. A* **270**, 172 (1962).

[88] M. Blume and R. E. Watson. *Proc. Roy. Soc. A* **271**, 565 (1963).

[89] M. Blume, A. Freeman, and R. E. Watson. *Phys. Rev. A* **272**, 320 (1964).

[90] B. A. Hess, C. M. Marian, U. Wahlgren, and O. Gropen. *Chem. Phys. Lett.* **251**, 365 (1996).

[91] B. Schimmelpfennig. *Atomic Spin-Orbit Mean-Field Integral (AMFI) Program* (Stockholms Universitet, Stockholm, 1996).

[92] W. Kutzelnigg. *Theor. Chem. Acc.* **73**, 173 (1988).

[93] N. F. Ramsey. *Phys. Rev.* **77**, 567 (1950).

[94] N. F. Ramsey. *Phys. Rev.* **78**, 699 (1950).

[95] N. F. Ramsey. *Phys. Rev.* **83**, 540 (1951).

[96] N. F. Ramsey. *Phys. Rev.* **86**, 243 (1952).

[97] J. Olsen and P. Jorgensen. *J. Chem. Phys.* **82**, 3235 (1985).

[98] R. McWeeny. *Methods of Molecular Quantum Mechanics.* 2nd ed. (Academic, London, 1992).

[99] P. Belanzoni, E. J. Baerends, S. van Asselt, and P. B. Langewen. *J. Phys. Chem.* **99**, 13094 (1995).

[100] A. V. Arbuznikov, J. Vaara, and M. Kaupp. *J. Chem. Phys.* **120**, 2127 (2004).

[101] F. Neese. *J. Chem. Phys.* **127**, 164112 (2007).

[102] F. Neese. *ORCA, versions 2.6.4 and 2.6.35* (University of Bonn, 2007-2008).

[103] J. Vaara, K. Ruud, O. Vahtras, H. Ågren, and J. Jokisaari. *J. Chem. Phys.* **109**, 1212 (1998).

[104] R. J. Kurland and B. R. J. McGarvey. *J. Magn. Reson.* **2**, 286 (1970).

[105] V. Barone, P. Cimino, and A. Pedone. *Magn. Reson. Chem.* **48**, S11 (2010).

[106] P. Manninen and J. Vaara. *Phys. Rev. A* **69**, 022503 (2004).

[107] J. Vaara, P. Manninen, and J. Lounila. *Chem. Phys. Lett.* **372**, 750 (2003).

[108] G. Pagola, M. Caputo, M. Ferraro, and P. Lazzeretti. *J. Chem. Phys.* **120**, 9556 (2004).

[109] E. Tellgren, A. Soncini, and T. Helgaker. *J. Chem. Phys.* **129**, 154114 (2008).

[110] M. Kaupp and F. H. Köhler. *Coord. Chem. Rev.* **253**, 2376 (2009).

[111] H. Heise, F. H. Köhler, F. Mota, J. J. Novoa, and J. Veciana. *J. Am. Chem. Soc.* **121**, 9659 (1999).

[112] A. D. Becke. *J. Chem. Phys.* **98**, 5648 (1993).

[113] P. J. Stephens, F. J. Devlin, C. F. Chabalowski, and M. J. Frisch. *J. Phys. Chem.* **98**, 11623 (1994).

[114] See http://www.theochem.uni-stuttgart.de/pseudopotentials/index.html.

[115] K. Wolinski, J. F. Hinton, and P. Pulay. *J. Am. Chem. Soc.* **112**, 8251 (1990).

[116] K. Ruud, B. Schimmelpfennig, and H. Ågren. *Chem. Phys. Lett.* **310**, 215 (1999).

[117] J. Vaara, O. L. Malkina, H. Stoll, V. G. Malkin, and M. Kaupp. *J. Chem. Phys.* **114**, 61 (2001).

[118] F. Neese. *J. Chem. Phys* **122**, 034107 (2005).

[119] D. Ganyushin and F. Neese. *J. Chem. Phys.* **125**, 024103 (2006).

[120] R. Reviakine, A. Arbuznikov, J.-C. Tremblay, C. Remenyi, O. L. Malkina, I. Malkin, and M. Kaupp. *J. Chem. Phys.* **125**, 054110 (2006).

[121] M. Enders, P. Fernández, G. Ludwig, and H. Pritzkow. *Organometallics* **20**, 5005 (2001).

[122] M. P. Allen and D. J. Tildesley. *Computer Simulation of Liquids* (Clarendon Press, Oxford, 1987).

[123] C. van Wüllen. *J. Chem. Phys.* **130**, 194109 (2009).

[124] M. F. Rettig and R. S. Drago. *J. Am. Chem. Soc.* **91**, 1361 (1969).

[125] M. F. Rettig and R. S. Drago. *Chem. Comm.* 891 (1966).

[126] J. Blümel, M. Herker, W. Hiller, and F. H. Köhler. *Organometallics* **15**, 3474 (1996).

[127] F. H. Köhler and X. Xie. *Magn. Reson. Chem.* **35**, 487 (1997).

[128] A. D. Becke. *Phys. Rev.* **38**, A3098 (1988).

[129] J. P. Perdew. *Phys. Rev.* **33**, B8822 (1986).

[130] J. P. Perdew, K. Burke, and M. Ernzerhof. *Phys. Rev. Lett.* **77**, 3865 (1996). Erratum: Phys. Rev. Lett. **78**, 1386 (1997).

[131] C. Lee, W. Yang, and R. G. Parr. *Phys. Rev. B* **37**, 785 (1988).

[132] A. D. Becke. *J. Chem. Phys.* **98**, 1372 (1993).